
BACHELORARBEIT

# Time Domain Perfectly Matched Layers in Generalized Star-shaped Domains for Scalar Problems

ausgeführt am

Institut für
Analysis und Scientific Computing
TU Wien

unter der Anleitung von

**Assoc. Prof. Dr. Lothar Nannen**

durch

**Constantin Pierer**
Matrikelnummer: 12209454
Hochstraße 48
2380 Perchtoldsdorf

Wien, am 26. Oktober 2025

## Abstract

Modeling wave-like phenomena poses significant mathematical complications, when regarding an unbounded domain. In order to apply standard finite element methods, it is necessary to truncate the computational grid in some way. However difficulties arise, since typically solutions of the wave equation are inherently non-local. This means that even a small excitation can propagate over a large region. Thus, a simple truncation with hard-wall boundary conditions (e.g. Dirichlet or Neumann), will cause unacceptable reflections propagating into the computational domain. Therefore, wave equations on unbounded domains require different approaches.

The technique of *complex scaling* is a popular choice when treating such problems. First, the Fourier transformation is applied, which transforms the system from the time domain into the frequency domain. This allows to introduce a complex coordinate transformation outside of a chosen domain of interest, which is done to ensure artificial damping of the wave without spurious reflections. When using so called *Perfecly Matched Layers*, the exterior domain (i.e, the subdomain where the complex scaling is introduced) is truncated and discretized with finite element methods. Then again, applying the inverse Fourier transformation yields the corresponding system in the time domain. Common choices for these complex scalings are the so called *cartesian scaling* and *radial scaling*. Depending on the application, especially the geometry at hand, one approach may be more suitable than the other. In this work, we introduce a generalization of these methods, amenable to applications on star-shaped domains. Based on findings of [Wes20], we introduce specific complex transformations and develop the corresponding formulation in the time domain to solve source problems. Concerning the discretization of the problem, we follow the approach of decomposing a wave into an oscillating transversal and a propagating radial part. This decomposition allows a quick adaptation of our method to specific geometries at hand. Moreover, this particular approach avoids the need of explicit meshing of the exterior domain, and can therefore be easily implemented into regular finite element software (e.g. netgen/ngsolve [Sch14; Sch97]).

The work of [RSS12] reported the occurrence of numerical instabilities in the simulation of wave phenomena in open systems, which were not fully understood at the time. In the present study, we provide a theoretical idea for these instabilities by analyzing their underlying mechanisms within our framework. Furthermore, we apply our proposed method to the same setting and demonstrate that it remains stable and robust, supported by numerical tests.

# Acknowledgment

First and foremost, I would like to express my sincere gratitude to my advisor, Assoc. Prof. Lothar Nannen, and my co-advisor, Dipl.-Ing. Dr. techn. Markus Wess, for their invaluable support throughout the past months. Regardless of the question, you always took the time to sit down with me and explain every detail patiently. Not a single discussion ever felt like a setback — your guidance, and encouragement consistently helped me move forward. Thank you for giving me the opportunity to work on such an interesting topic. It has truly sparked my interest in numerical analysis, and I look forward to the possibility of collaborating with you again in the future.

I also want to thank my parents who were the first to support me and thankfully never stopped doing so ever since. Without your help, I couldn't have pursued my passion for studying mathematics over the last 3 years. My sisters — Antonia, Valentina, and Sophie — have never stopped supporting me either, whose contributions range from helping me keeping my sanity during the last 3 years, to giving me advice in difficult situations beyond mathematics.

Most importantly, I want to thank my friends from university. It is you who make studying enjoyable, even in difficult times. I believe that the German proverb „Geteiltes Leid ist halbes Leid“ captures our spirit best. I can't remember a single situation in which any of you refused to help when help was needed. You will always have a special place in my heart. Thank you!

26. Oktober 2025 Constantin Pierer

# Eidesstattliche Erklärung

Ich erkläre an Eides statt, dass ich die vorliegende Bachelorarbeit selbstständig und ohne fremde Hilfe verfasst, andere als die angegebenen Quellen und Hilfsmittel nicht benutzt bzw. die wörtlich oder sinngemäß entnommenen Stellen als solche kenntlich gemacht habe.

Wien, am 26. Oktober 2025

Constantin Pierer

# Inhaltsverzeichnis

# 1. Introduction

In numerous physical and engineering applications, wave phenomena can be modeled mathematically by partial differential equations (PDEs). In standard scenarios the objective equation, the so called *wave equation*, is given by,

$$\partial_{tt} p(\mathbf{x}, t) - \Delta_{\mathbf{x}} p(\mathbf{x}, t) = f(\mathbf{x}, t). \tag{1.1}$$

Here $p$ describes the unknown wave function and f is a given source term. A typical example is the modeling of surface water waves, in which $p$ corresponds to the deviation of the water surface. Modeling wave-type scenarios on bounded domains is fairly straight forward, (see [Eva10]). However, when trying to simulate wave propagation on open domains, many difficulties arise. In order to apply standard finite element methods we need to truncate the computational domain, where the key questions lies in how to perform this truncation. As wave solutions usually exhibit oscillating behavior coupled with an asymptotic behavior $\sim 1/r^{(d-1)/2}$, for distance $r$ and dimension $d$ (see, [Joh21]), truncating the domain and imposing hard-wall boundary conditions such as Neumann or Dirichlet, will lead to unacceptable artifacts. However, choosing a time harmonic Ansatz of the form

$$p(\mathbf{x}, t) = \Re(u(\mathbf{x}) \exp(-i\omega t)), \tag{1.2}$$

for a fixed frequency $\omega$, and insertion into (1.1), results in the so called *Helmholtz equation*,

$$-\Delta u(\mathbf{x}) - \omega^2 u(\mathbf{x}) = f(\mathbf{x}). \tag{1.3}$$

The advantage of working in the frequency domain is that conditions and transformations can be imposed more easily, as the equation is expressed only in spatial dimensions. Complex scaling techniques in the frequency domain (see, e.g. [Sim79]) have been developed prior to the time-dependent *Perfectly Matched Layer (PML)* method introduced by Bérenger in [Ber94]. However, these methods were later recognized to be equivalent when written in the frequency domain.

The key point of these approaches lies in introducing a complex coordinate transformation outside the chosen domain of interest. This scaling ensures that within the interior domain, the wave remains unchanged, however, within the exterior domain, the subdomain where the transformation is introduced, the solution exhibits an artificially damped behavior. Common choices of scalings are the so called *cartesian scaling* and *radial scaling* (see, e.g. [BP13] and [HKW24], [Hal19]), but as their names already suggest, they only work properly on specific geometries. In chapter 3 and 4 we discuss well-known approaches in simple frameworks and focus specifically on the *cartesian scaling* in greater detail. However, [Wes20] presents detailed findings for complex scalings for the Helmholtz problem, even for more general geometries. In chapter 5 and 6 we built upon these findings, pick specific scaling parameters and adapt

this approach in order to solve the open domain source problem. For the discretization, we employ a formulation that decomposes the wave into an oscillatory transverse component and a radially propagating component. This representation provides a physically meaningful framework that can be efficiently adapted to various geometrical configurations. In the final chapter 7, we support our results by numerical test and furthermore return to the setting studied in [RSS12], explain the origin of the instabilities observed there, and apply our method to demonstrate its robustness and stability.

# 2. Classical approaches for the Wave Equation

The wave equation is a fundamental model for prescribing wave propagation phenomena in various physical systems. Typically one is interest in the behavior of the wave over time, given an initial state, specified by $p_0$ and $p_1$. The corresponding equations to be solved can be formulated as,

$$\begin{aligned}
\partial_{tt} p(\mathbf{x},t) - \Delta_{\mathbf{x}} p(\mathbf{x},t) &= 0, && \mathbf{x} \in \Omega,\ t > t_0, && \text{(2.1a)}\\
p(\mathbf{x},t) \text{ satisfies suitable boundary conditions}, && \mathbf{x} \in \partial\Omega,\ t > t_0, && \text{(2.1b)}\\
p(\mathbf{x},t_0) &= p_0(\mathbf{x}), && \mathbf{x} \in \Omega, && \text{(2.1c)}\\
\partial_t p(\mathbf{x},t_0) &= p_1(\mathbf{x}), && \mathbf{x} \in \Omega. && \text{(2.1d)}
\end{aligned}$$

We do not specify the type of boundary conditions (e.g., Dirichlet or Neumann), as the analysis remains valid in both cases. However, the initial conditions $p_0$ and $p_1$ are assumed to be compatible with the prescribed boundary conditions. The choice of an appropriate approximation method for solving (2.1) may vary with the characteristics of the domain $\Omega$, particularly its size.

## 2.1. Bounded Domains

If $\Omega$ is a bounded domain, and given that both $\partial\Omega$ and the initial data are sufficiently smooth, then (2.1) is uniquely solvable (e.g. [Eva10]), making it amenable to classic numerical methods. In particular, well known approaches such as finite element methods (FEM) combined with time-stepping schemes are commonly used (see, [IMN+25, Section 7.4 - 7.5]) to approximate a solution.

Proceeding with the classical FEM procedure (see, [MF24, Section 3.2]), we rewrite (2.1) into variational formulation and approximate it with spatial basis functions. Further, order-reduction leads to the following first order system of differential equations,

$$\begin{aligned}
M\dot{q}(t) + Sp(t) &= 0, && \forall\, t \geq t_0,\\
\dot{p}(t) &= q(t), && \forall\, t \geq t_0,\\
p(t_0) &= p_0,\\
q(t_0) &= p_1.
\end{aligned} \tag{2.2}$$

One frequently used time stepping scheme to solve (2.2) is the so called *Crank-Nicolson*.

**Algorithm A (Crank–Nicolson scheme for first-order wave system).**
*At each time step with step size $\tau > 0$:*
*Solve:*

$$M\left(\frac{q^{n+1} - q^n}{\tau}\right) + S\left(\frac{p^{n+1} + p^n}{2}\right) = 0,$$

$$\frac{p^{n+1} - p^n}{\tau} = \frac{q^{n+1} + q^n}{2}.$$

A key feature of Algorithm A is its ability to conserve the energy of the system over time. This energy preservation ensures stable and physically meaningful solutions.

## 2.2. Unbounded Domains

With unbounded domains $\Omega$, on the other side, some issues arise when trying to approach these problems similarly to the bounded case. Since standard FEM is applicable only on bounded regions, it is rather challenging to model wave-like behavior on unbounded regions.

One common approach to analyze wave-type equations is to use a time-harmonic ansatz,

$$p(t, \mathbf{x}) = \Re(u(\mathbf{x}) \exp(-i\omega t)), \tag{2.3}$$

for a frequency $\omega$. Plugging this Ansatz into (2.1a) leads to the (homogeneous) *Helmholtz equation*,

$$-\Delta u(\mathbf{x}) - \omega^2 u(\mathbf{x}) = 0, \qquad \mathbf{x} \in \Omega, \tag{2.4a}$$

$$u \text{ fulfills some boundary conditions}, \qquad \mathbf{x} \in \partial\Omega, \tag{2.4b}$$

$$u \text{ is radiating}, \qquad \|\mathbf{x}\| \to \infty. \tag{2.4c}$$

Now as this equation is independent of the time, we refer to it as a equation in the *frequency domain*. This approach is very common for modeling waves on unbounded domains, since in the frequency domain it is possible to impose so called radiation conditions.

Since $\Omega$ is unbounded, (2.4c) compensates for the missing boundary conditions. At this point, we require radiation conditions in order to guarantee physically meaningful solutions. In one dimension their meaning is rather intuitive.

In this case, the direction of propagation is unique, however, there exist so called *scattered* (outgoing) and *incoming* solutions. Since incoming waves, are physically not meaningful, one has to pose conditions in order to guarantee the solution only consists of scattering parts (see, [Wes20, Section 2.2]). However, in higher dimensions the concept of radiation conditions is non trivial, especially in the context of finite element approximation. That is why we refer to [Wes20, Section 2.2] for more detail.

Although these issues arise, we mostly overcome them by applying the technique of complex scaling. Through applying specific coordinate transformations, we alter the solution outside the domain of interest in a way, that artificial reflections are avoided. In the following chapters we will specify the tools for this approach mathematically, in order to then implement and test them.

# 3. Perfectly Matched Layers in the Frequency Domain

A frequently used technique to model wave phenomena on open or unbounded domains by absorbing outgoing waves, is called *Perfectly Matched Layers*. We will now clarify the principle of absorption and start by focusing on the one dimensional framework to make the concepts more intuitive and easier to grasp.

## 3.1. PMLs in one dimension

Consider the one dimensional Helmholtz problem for a given $\omega > 0$ with $a > 0$ such that f is compactly supported in the interval $(0, a)$. We aim to find $u : (0, \infty) \to \mathbb{R}$ such that,

$$-u'' - \omega^2 u = f, \tag{3.1a}$$

$$u(0) = 0, \tag{3.1b}$$

$$\lim_{x\to\infty} u'(x) - i\omega u(x) = 0. \tag{3.1c}$$

The last condition (3.1c) is the so called *Sommerfeld radiation condition (SRC)*. It compensates for the missing boundary condition at the right and guarantees physically reasonable solutions, namely solutions that only consist of outgoing waves. The Sommerfeld radiation condition represents a particular case of the radiation conditions. For more detail regarding the SRC we refer to [CK13, Section 2.1].

The general solution to (3.1a) is given by,

$$u(x) = \varphi(x, a)\exp(i\omega x) + \psi(x, a)\exp(-i\omega x), \tag{3.2}$$

for some $\varphi, \psi$. Note that the $\exp(-i\omega x)$ term corresponds to an unwanted incoming wave for $x \geq a$. Inserting the boundary conditions yields for $x \geq a$ a solution of the form,

$$u(x) = c\exp(i\omega x), \quad c \in \mathbb{C}.$$

One now observes that u allows for $x \geq a$ a holomorphic extension to $\mathbb{C}$. Hence we can introduce a complex scaling,

$$\tilde{x}(x) := \begin{cases} x, & x < a, \\ x + i\alpha(x - a), & x \geq a, \end{cases} \tag{3.3}$$

with $\alpha > 0$.

For $\tilde{u}(x) := u(\tilde{x}(x))$ we obtain,

$$\tilde{u}(x) = c\exp(-\alpha\omega(x-a))\exp(i\omega x), \quad x \geq a. \tag{3.4}$$

Ultimately we have altered the solution to (3.1) such that it remains unchanged in $(0, a)$ and decreases exponentially along the curve $x \mapsto \tilde{x}(x)$. The altered solution $\tilde{u}$ is precisely what we refer to as a damped solution. The variational formulation to find $\tilde{u} \in H_0^1(0,\infty)$ is given by,

$$\int_0^a \tilde{u}'\hat{u}' + \frac{1}{1+i\alpha}\int_a^\infty \tilde{u}'\hat{u}' - \omega^2\int_0^a \tilde{u}\hat{u} - \omega^2(1+i\alpha)\int_a^\infty \tilde{u}\hat{u} = \int_0^a f\hat{u}, \tag{3.5}$$

for all $\hat{u} \in H_0^1(0,\infty)$.
In order to make (3.5) amenable to FEM discretizations, we truncate the domain to (0,T) for some sufficiently large $T > a$ and impose homogeneous Neumann or Dirichlet boundary conditions at x = T. We expect an exponentially small truncation error, since the solution decreases exponentially for $x \to \infty$. [NW22; Hal21].

## 3.2. PMLs in higher dimensions

In higher dimensions we follow the same formula as in the one dimensional case. We try to decompose the solution to the Helmholtz equation and transform it in a way so that it decays exponentially. However, the situation gets more complicated, since in free space $\mathbb{R}^2$ the direction of propagation is not unique.

We start by decomposing the solution into modes and transforming into polar coordinates with $x = r\hat{x}, r > 0, \hat{x} \in B_1(0)$,

$$u(r\hat{x}) = \sum_{n=-\infty}^{\infty} (c_{1,n}H_{|n|}^{(1)}(\omega r) + c_{2,n}H_{|n|}^{(2)}(\omega r))\Phi_n(\hat{x}).$$

Where $H_n^{(1)}$ and $H_n^{(2)}$ are the cylindrical Hankel functions of the first and second kind, respectively and $\Phi_n$ are the cylindrical harmonics.

The Hankel functions have a nice asymptotic behaviour (see e.g. [Wes20, Proposition A.3], namely,

$$H_n^{(1,2)}(z) \approx \sqrt{\frac{2}{\pi z}}\exp(\pm i(z - \frac{\pi n}{2} + \frac{\pi}{4})). \tag{3.6}$$

The Hankel functions of the first kind correspond to the outgoing waves, while those of the second kind correspond to the unwanted incoming waves. That is why they can be interpreted as the two dimensional generalization of the exponentials, from the one dimensional framework.

According to [Wes20, Proposition 2.8] the radiation condition yields the solution,

$$u(r\hat{x}) = \sum_{n=-\infty}^{\infty} c_n H_{|n|}^{(1)}(\omega r)\Phi_n(\hat{x}),$$

for $r > r_0$ such that all sources and obstacles are contained in the ball $B_{r_0}(0)$.

We will now introduce specific complex transformations $\tilde{\mathbf{x}}(\mathbf{x})$, in order to get an exponentially decreasing solution. To achieve this behavior, it is essential that that the transformation $\mathbf{x} \mapsto \tilde{\mathbf{x}}(\mathbf{x})$ satisfies the property $\Im(\tilde{\mathbf{x}}(\mathbf{x})) \to \infty$ for $|\mathbf{x}| \to \infty$.

## 3.3. Cartesian scaling

A particular popular choice, due to its straight forward implementation, is the cartesian scaling method. The idea is to scale linearly in x and y direction to obtain $\tilde{\mathbf{x}}(\mathbf{x})$. Assume all sources and inhomogeneties are contained in the box $\Omega_{\text{int}} = (a_0, a_1) \times (b_0, b_1)$. We define for some $\alpha > 0$ the complex scaling into $\Omega_{\text{ext}} = \Omega \setminus \Omega_{\text{int}}$ as,

$$\begin{aligned} \tilde{\mathbf{x}}(\mathbf{x}) &= \begin{pmatrix} \tilde{x} \\ \tilde{y} \end{pmatrix} \left( (x, y)^\top \right) \\ &= \begin{pmatrix} x \\ y \end{pmatrix} + i\alpha \begin{pmatrix} (x - a_1)\chi_{x>a_1}(x) + (x - a_0)\chi_{x<a_0}(x) \\ (y - b_1)\chi_{y>b_1}(y) + (y - b_0)\chi_{y<b_0}(y) \end{pmatrix}. \end{aligned} \tag{3.7}$$

where $\chi_{x>a}$ notates the characteristic function of the set $\{x : x > a\}$.

Denote by $\tilde{u}(\mathbf{x}) := u(\tilde{\mathbf{x}}(\mathbf{x}))$ the complex scaled solution of the Helmholtz equation and by $J_{\tilde{\mathbf{x}}}$ the Jacobian matrix of the scaling $\tilde{\mathbf{x}}$. Then $\tilde{u} \in H^1(\mathbb{R}^d)$ satisfies,

$$\int_{\Omega_{\text{int}}} \nabla\tilde{u} \cdot \nabla\hat{u} + \int_{\Omega_{\text{ext}}} (J_{\tilde{\mathbf{x}}}^{-\top} \nabla\tilde{u}) \cdot (J_{\tilde{\mathbf{x}}}^{-\top} \nabla\hat{u}) \det J_{\tilde{\mathbf{x}}} - \omega^2 \int_{\Omega_{\text{int}}} \tilde{u}\hat{u} - \omega^2 \int_{\Omega_{\text{ext}}} \tilde{u}\hat{u} \det J_{\tilde{\mathbf{x}}} = \int_{\Omega_{\text{int}}} f\hat{u}, \tag{3.8}$$

for all $\hat{u} \in H^1(\mathbb{R}^2)$.

To implement the PML formulation, the Jacobian Matrix of the mapping $\tilde{\mathbf{x}}$ is needed, which is given by,

$$J\left((x, y)^\top\right) = \mathbf{I} + i\alpha \begin{pmatrix} \chi_{x<a_0}(x) + \chi_{x>a_1}(x) & 0 \\ 0 & \chi_{y<b_0}(y) + \chi_{y>b_1}(y) \end{pmatrix}, \tag{3.9}$$

where $\mathbf{I}$ denotes the identity matrix. [BP13; NW22]

### 3.3.1. Parameter sensitivity analysis

The challenging aspect lies in the choice of the PML parameters, especially in selecting $\alpha$ suitably, as it directly influences the convergence rate of the scaled solution. Choosing just a single parameter poorly, can lead to a bad resolution. One can distinguish between two primary error sources.

On one hand choosing $\alpha$ too small will lead to slowly decreasing solutions, which allows unwanted incoming waves, since artificial reflections at the boundaries $\partial\Omega_{\text{ext}}$ are created. On the other hand, choosing $\alpha$ too large results in poor resolution of the solution near the boundary region between $\Omega_{\text{ext}}$ and $\Omega_{\text{int}}$. Since the scaled solution exhibits oscillatory

behavior in $\Omega_{\text{int}}$ and decays exponentially in $\Omega_{\text{ext}}$, numerical inaccuracies are particularly likely to occur in this intermediate region. Moreover, such errors can propagate throughout the entire domain, ultimately degrading the overall quality of the solution. In the following we will examine how both $\alpha$ and the order of the finite element basis function, influence the quality of the (approximated) solution of (3.8). To be precise, we aim to approximate the solution of (3.8), using a Gaussian point source as the right-hand side, for various PML parameters. All model parameters are summarized in Table 1.

We select $\alpha = 1$ as the parameter for the reference solution, as it yields a stable and convergent result with high resolution near the boundaries. Figure 1a illustrates how the complex scaling preserves for the reference solution a natural, wave-like behavior within the domain $\Omega_{\text{int}}$ and guarantees absorption within $\Omega_{\text{ext}}$. Figure 1b further demonstrates the exponential decay of the solution within the PML region $\Omega_{\text{ext}}$, illustrated along a horizontal cross-section in the x-direction.

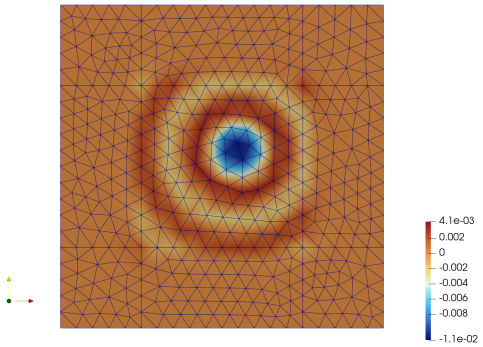


(a) Real part of reference solution.

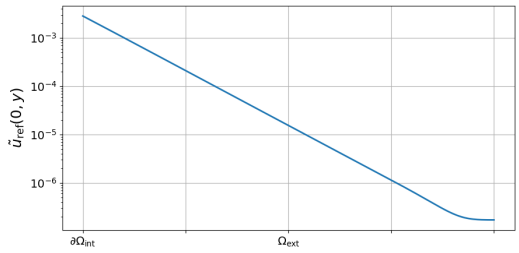


(b) Exponential decay of reference solution in $\Omega_{\text{ext}}$.

Figure 1.: Behavior of the reference solution

We now investigate how solutions obtained with different PML parameters behave in comparison to the reference solution. Figure 2 shows the relative $H^1$-error in $\Omega_{\text{int}}$ for various FEM orders and different values of $\alpha$. The plot provides a clear representation of the previously discussed error terms. We can see that both overly small and excessively large choices of $\alpha$ result in increased errors. However, if the parameter is only slightly overestimated, the resulting error can be mitigated by using a higher order FEM space. This approach is reasonable if the PML layer is relatively thin.

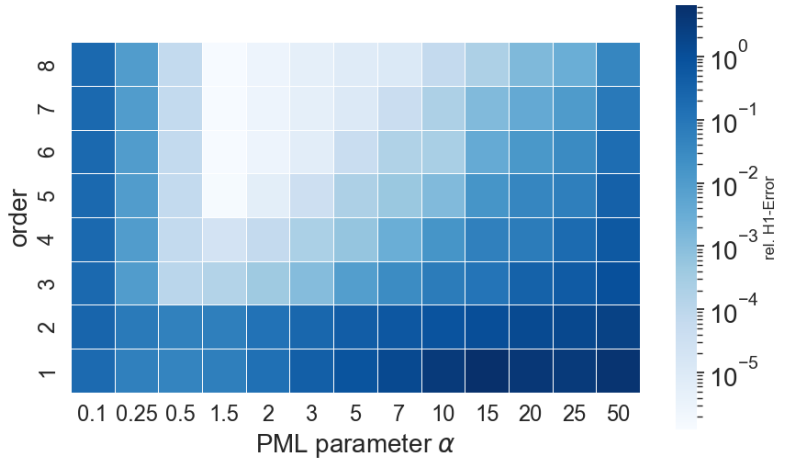


Figure 2.: relative $H_1$-error in $\Omega_{\text{int}}$ for various PML parameters.

# 4. Perfectly Matched Layers in the Time domain

As we have briefly discussed in section 2.2, the wave equation and the Helmholtz equation are coupled together through the (inverse) Fourier transformation. In chapter 3 we focused only on positive frequency numbers $\omega$. This does not pose a problem in the frequency domain, since we can simply choose $\omega > 0$. However, in order to go back to the time domain, we need to apply the inverse Fourier transformation, which includes an integral over the entire real axis with respect to $\omega$ (see, A.1). Therefore, simply replacing the factors of $-i\omega$ by time derivatives and solving the corresponding problem in the time domain will result in exponentially increasing solutions. This is because the PML imposes actually an incorrect radiation condition for negative frequency values. We try to avoid this problem by introducing a frequency dependent damping parameter.[Joh21]

## 4.1. Time domain PMLs in one dimension

Consider the frequency dependent damping parameter $\alpha(\omega) := \frac{\alpha_0}{\omega}$ for some $\alpha_0 > 0$. We begin by stating the general first-order variational Helmholtz equation.

Find $p \in H_0^1(0,\infty)$ and $v \in L_2(0,\infty)$, such that

$$-i\omega \int_0^a v\hat{v} - i\omega(1 + i\alpha_0/\omega) \int_a^\infty v\hat{v} - \int_0^\infty p'\hat{v} = \int_0^a f\hat{v}, \tag{4.1a}$$

$$-i\omega \int_0^a p\hat{p} - i\omega(1 + i\alpha_0/\omega) \int_a^\infty p\hat{p} + \int_0^\infty v\hat{p}' = 0. \tag{4.1b}$$

for all $\hat{p} \in H_0^1(0,\infty)$ and $\hat{v} \in L_2(0,\infty)$. It is useful to rewrite this into,

$$-i\omega \int_0^\infty v\hat{v} = -\alpha_0 \int_a^\infty v\hat{v} + \int_0^\infty p'\hat{v} + \int_0^a f\hat{v}, \tag{4.2a}$$

$$-i\omega \int_0^\infty p\hat{p} = -\alpha_0 \int_a^\infty p\hat{p} - \int_0^\infty v\hat{p}'. \tag{4.2b}$$

Since (4.2) depends explicitly on the sign of $\omega$, this formulation ensures correct outgoing solutions for both positive and negatives values of $\omega$. Therefore, applying the inverse Fourier transformation leads to the following system, which now also provides exponentially damped

solutions,

$$\partial_t \int_0^\infty v\hat{v} = -\alpha_0 \int_a^\infty v\hat{v} + \int_0^\infty \partial_x p\, \hat{v} + \int_0^a f\hat{v}, \tag{4.3a}$$

$$\partial_t \int_0^\infty p\hat{p} = -\alpha_0 \int_a^\infty p\hat{p} - \int_0^\infty v\, \partial_x \hat{p}. \tag{4.3b}$$

We denote the functions in the time domain the same as the ones in the frequency domain. However, we equip the necessary time domain functions with homogeneous initial conditions at $t = 0$. Now again, to make (4.3) feasible for FEM discretizations, one has to truncate the domain to $(0, T)$ for some $T > a$ sufficiently large.

## 4.2. Time domain PMLs in higher dimensions

Now, we generalize the one dimensional framework and regard higher dimensions. This means, we aim to extend the idea of section 3.2 in a way, such that it works for all frequency numbers. Consequently, the corresponding equations are transformed back into the time domain.

As usual, we start with the first-order variational Helmholtz equation for bounded $\Omega$.

Find $p \in H_0^1(\Omega)$ and $v \in L_2(\Omega)^2$, such that

$$-i\omega \int_\Omega v \cdot \hat{v} - \int_\Omega \nabla p \cdot \hat{v} = \int_\Omega f\hat{v}, \tag{4.4a}$$

$$-i\omega \int_\Omega p\hat{p} + \int_\Omega v \cdot \nabla \hat{p} = 0. \tag{4.4b}$$

for all $\hat{p} \in H_0^1(\Omega)$ and $\hat{v} \in L_2(\Omega)^2$.

As done in chapter 3, we introduce a complex scaling $x \mapsto \tilde{\mathbf{x}}(x)$, which separates $\Omega$ into $\Omega_{\text{int}}$ and $\Omega_{\text{ext}}$. This yields,

$$-i\omega \int_\Omega v \cdot \hat{v} \det J_{\tilde{\mathbf{x}}} - \int_\Omega J_{\tilde{\mathbf{x}}}^{-\top} \nabla p \cdot \hat{v} \det J_{\tilde{\mathbf{x}}} = \int_{\Omega_{\text{int}}} f\hat{v}, \tag{4.5a}$$

$$-i\omega \int_\Omega p\hat{p} \det J_{\tilde{\mathbf{x}}} + \int_\Omega v \cdot J_{\tilde{\mathbf{x}}}^{-\top} \nabla \hat{p} \det J_{\tilde{\mathbf{x}}} = 0. \tag{4.5b}$$

where $J_{\tilde{\mathbf{x}}}$ denotes the Jacobian matrix of the complex mapping $\tilde{\mathbf{x}}$. One now observes that $J_{\tilde{\mathbf{x}}}$ possibly depends explicitly on $\omega$, therefore (4.5) might depend rationally on $-i\omega$. Ultimately, we want to apply the Fourier transformation to the system, but since these rational expression lead to convolution operators in time, we have to get rid of them. Usually this is done by introducing auxiliary functions. [Joh21; NW22]

## 4.3. Time domain Cartesian scaling

We start by replacing $v, \hat{v}$ with their Piola transform $v = \frac{1}{\det J_{\tilde{\mathbf{x}}}(\mathbf{x})} J_{\tilde{\mathbf{x}}}(\mathbf{x})\check{v}$ and $\hat{v} = \frac{1}{\det J_{\tilde{\mathbf{x}}}(\mathbf{x})} J_{\tilde{\mathbf{x}}}(\mathbf{x})\check{\hat{v}}$ in (4.5) to obtain,

$$-i\omega \int_\Omega \check{v} \cdot J_{\tilde{\mathbf{x}}}^\top J_{\tilde{\mathbf{x}}} \check{\hat{v}} \frac{1}{\det J_{\tilde{\mathbf{x}}}} - \int_\Omega \nabla p \cdot \hat{v} = \int_{\Omega_{\text{int}}} f\hat{v}, \tag{4.6a}$$

$$-i\omega \int_\Omega p\hat{p} \det J_{\tilde{\mathbf{x}}} + \int_\Omega \check{v} \cdot \nabla \hat{p} = 0. \tag{4.6b}$$

Similarly to the derivation in section (3.3), we compute the expressions $J_{\tilde{\mathbf{x}}}$ and $\det J_{\tilde{\mathbf{x}}}$ in (4.6) with $\alpha(\omega) := \frac{\alpha_0}{\omega}$.

$$J_{\tilde{\mathbf{x}}}(\mathbf{x}) = \begin{cases} \begin{pmatrix} 1 - \frac{\alpha}{i\omega} & 0 \\ 0 & 1 \end{pmatrix}, & \mathbf{x} \in \Omega_{lr}, \\ \begin{pmatrix} 1 & 0 \\ 0 & 1 - \frac{\alpha}{i\omega} \end{pmatrix}, & \mathbf{x} \in \Omega_{tb}, \\ \begin{pmatrix} 1 - \frac{\alpha}{i\omega} & 0 \\ 0 & 1 - \frac{\alpha}{i\omega} \end{pmatrix}, & \mathbf{x} \in \Omega_c, \\ I, & \mathbf{x} \in \Omega_{\text{int}}, \end{cases} \tag{4.7}$$

$$\det J_{\tilde{\mathbf{x}}}(\mathbf{x}) = \begin{cases} 1 - \frac{\alpha}{i\omega}, & \mathbf{x} \in \Omega_{lr} \cup \Omega_{tb}, \\ \left(1 - \frac{\alpha}{i\omega}\right)^2, & \mathbf{x} \in \Omega_c, \\ 1, & \mathbf{x} \in \Omega_{\text{int}}, \end{cases} \tag{4.8}$$

with

$$\begin{aligned} \Omega_{lr} &= \{(x,y) : x \in (a_0,a_1)^c, y \in (b_0,b_1)\}, \\ \Omega_{tb} &= \{(x,y) : x \in (a_0,a_1), y \in (b_0,b_1)^c\}, \\ \Omega_c &= \mathbb{R}^2 \setminus (\Omega_{\text{int}} \cup \Omega_{tb} \cup \Omega_{lr}), \\ \Omega_{\text{int}} &= \{(x,y) : x \in (a_0,a_1), y \in (b_0,b_1)\}. \end{aligned}$$

Further computations provide,

$$-i\omega \det J_{\tilde{\mathbf{x}}}(\mathbf{x}) = \begin{cases} -i\omega + \alpha, & \mathbf{x} \in \Omega_{lr} \cup \Omega_{tb}, \\ -i\omega + 2\alpha - \frac{\alpha^2}{i\omega}, & \mathbf{x} \in \Omega_c, \\ -i\omega, & \mathbf{x} \in \Omega_{\text{int}}, \end{cases} \tag{4.9}$$

and

$$-\frac{i\omega}{\det J_{\tilde{\mathbf{x}}}(\mathbf{x})} J_{\tilde{\mathbf{x}}}(\mathbf{x})^\top J_{\tilde{\mathbf{x}}}(\mathbf{x}) = \begin{cases} \begin{pmatrix} -i\omega+\alpha & 0 \\ 0 & -ik-\alpha+\frac{\alpha^2}{-i\omega+\alpha} \end{pmatrix}, & \mathbf{x}\in\Omega_{lr}, \\ \begin{pmatrix} -i\omega-\alpha+\frac{\alpha^2}{-i\omega+\alpha} & 0 \\ 0 & -i\omega+\alpha \end{pmatrix}, & \mathbf{x}\in\Omega_{tb}, \\ -i\omega I, & \mathbf{x}\in\Omega_{\text{int}}\cup\Omega_c. \end{cases} \tag{4.10}$$

In order to eliminate the unwanted fractions of $-i\omega$, which would otherwise lead to convolution or integral operators in the time domain, we introduce two auxiliary functions k and z that satisfy,

$$-i\omega\int_{\Omega_c} k\hat{k} = \alpha^2\int_{\Omega_c} p\hat{k}, \qquad \forall \hat{k}\in H^1(\Omega_c), \tag{4.11}$$

$$-i\omega\int_{\Omega_{tb}\cup\Omega_{lr}} z\cdot\hat{z} = \alpha^2\int_{\Omega_{tb}\cup\Omega_{lr}} \check{v}\cdot\hat{z} - \alpha\int_{\Omega_{tb}\cup\Omega_{lr}} z\cdot\hat{z}, \qquad \forall \hat{z}\in H^1(\Omega_{tb}\cup\Omega_{lr})^2. \tag{4.12}$$

Altogether, this yields a system that allows us to conveniently transform it back into the time domain, which is then given by,

$$\begin{aligned}
&\partial_t\int_\Omega \check{v}\cdot\check{\hat{v}} = -\alpha\int_{\Omega_{lr}} \check{v}\cdot nn^\top\cdot\check{\hat{v}} + \alpha\int_{\Omega_{lr}} \check{v}\cdot(I-nn^\top)\cdot\check{\hat{v}} - \int_{\Omega_{lr}} z\cdot(I-nn^\top)\cdot\check{\hat{v}} \\
&+\alpha\int_{\Omega_{tb}} \check{v}\cdot nn^\top\cdot\check{\hat{v}} - \int_{\Omega_{tb}} z\cdot nn^\top\cdot\check{\hat{v}} - \alpha\int_{\Omega_{tb}} \check{v}\cdot(I-nn^\top)\cdot\check{\hat{v}} + \int_\Omega \nabla p\cdot\hat{v} - \int_{\Omega_{\text{int}}} f\hat{p}, \\
&\partial_t\int_\Omega p\hat{p} = -\alpha\int_{\Omega_{lr}\cup\Omega_{tb}} p\hat{p} - 2\alpha\int_{\Omega_c} p\hat{p} - \int_{\Omega_c} k\hat{p} - \int_\Omega \check{v}\cdot\nabla\hat{p}, \\
&\partial_t\int_{\Omega_c} k\hat{k} = \alpha^2\int_{\Omega_c} p\hat{k}, \\
&\partial_t\int_{\Omega_{tb}\cup\Omega_{lr}} z\cdot\hat{z} = \alpha^2\int_{\Omega_{tb}\cup\Omega_{lr}} \check{v}\cdot\hat{z} - \alpha\int_{\Omega_{tb}\cup\Omega_{lr}} z\cdot\hat{z}.
\end{aligned} \tag{4.13}$$

where,

$$n = \begin{cases} (1,0)^\top, & \Omega_{lr}, \\ (0,1)^\top, & \Omega_{tb}. \end{cases}$$

Note that we use the same symbols for the time domain functions as for the frequency domain ones. We only equip the necessary time domain functions with homogeneous initial values at $t = 0$. This system corresponds to the standard form of a damped wave equation in the time domain. It can be numerically approximated using suitable time-stepping schemes, such as finite difference or Runge-Kutta methods, depending on the desired accuracy and stability requirements. [IMN+25]

# 5. Generalized problem formulation and discretization

In the following chapter, we focus mainly on deriving a precise formulation of the Helmholtz problem and discussing how to discretize it in a reasonable way. Consequently we will derive different discretizations for both, the exterior and the interior part of the domain and finally couple them again. We have already seen in chapter 3 and 4 that the complex mapping $\mathbf{x} \mapsto \tilde{\mathbf{x}}(\mathbf{x})$ determines the interior subdomain $\Omega_{\text{int}}$ and the exterior subdomain $\Omega_{\text{ext}}$ heavily. We therefore start by introducing the exterior coordinates in a more general way. Throughout the whole chapter we will closely follow the approaches presented in [NW22, Section 3] and [Wes20, Section 6]. Furthermore, we assume from now on that the conditions from A.2 are satisfied.

## 5.1. Complex scaling into exterior coordinates

Following the definition as in [Wes20, Definition 3.1], we begin with recalling the concept of *(complex scaled) exterior coordinates.*

**Definition 5.1.** *Let $\Omega, \Omega_{\text{int}}, \Omega_{\text{ext}}, \Gamma \subset \mathbb{R}^2$ be such that A.2 is fulfilled. Moreover, let $\mathbf{v} : \Gamma \to \mathbb{R}^d$ be continuous and piecewise smooth.*

*(C1) the mapping*

$$\Psi : \begin{cases} \mathbb{R}_{>0} \times \Gamma \to \Omega_{\text{ext}}, \\ (\xi, \hat{\mathbf{x}}) \mapsto \hat{\mathbf{x}} + \xi \mathbf{v}(\hat{\mathbf{x}}), \end{cases} \tag{5.1}$$

*is a bijection.*

*Then we call the mapping $\Psi$ an* exterior coordinatization *of $\Omega_{\text{ext}}$. The mappings $\xi, \check{\mathbf{x}}$, given by*

$$(\xi(\mathbf{x}), \hat{\mathbf{x}}(\mathbf{x})) := \Psi^{-1}(\mathbf{x}),$$

are called exterior coordinates.

In our definition we omitted some conditions since they are satisfied in standard cases. For more detail we refer to [Wes20, Chapter 3].

Since we want to apply a complex scaling to star-shaped domains, we use Definition 5.1 to define complex scalings into exterior coordinates. For us the most important framework is in the context of star-shaped domains. Here $\mathbf{v}$ is definied as $\mathbf{v}(\tilde{\mathbf{x}}) := \tilde{\mathbf{x}} - \mathbf{m}$, where $\mathbf{m}$ denotes a chosen star-shaped center of $\Omega_{\text{int}}$.

**Definition 5.2.** *Let $\Omega$, $\Omega_{\text{int}}$, $\Omega_{\text{ext}}$, $\Gamma$ and $\Psi$, $\mathbf{v}$ be as in Definition 5.1. Then, for $\sigma \in \mathbb{C} \setminus \{0\}$, we define the mapping*

$$\Psi^\sigma : \begin{cases} \mathbb{R}_{>0} \times \Gamma \to \mathbb{C}^2, \\ (\xi, \hat{\mathbf{x}}) \mapsto \hat{\mathbf{x}} + \sigma \xi \mathbf{v}(\hat{\mathbf{x}}), \end{cases} \tag{5.2}$$

*and call $\Psi^\sigma(\mathbb{R}_{>0}, \Gamma)$ the* complex-scaled exterior domain.

Since the complex scaled solution is exponentially decaying and therefore square-integrable, we can pose the weak formulation of the (complex scaled) Helmholtz problem. Thus, we define the following (bi)-linear forms,

$$\begin{aligned}
m_{\text{int}}(\varphi, \psi) &:= \int_{\Omega_{\text{int}}} \varphi(x)\, \psi(x)\, \mathrm{d}x, \\
s_{\text{int}}(\varphi, \psi) &:= \int_{\Omega_{\text{int}}} \nabla\varphi(x) \cdot \nabla\psi(x)\, \mathrm{d}x, \\
m^\sigma_{\text{ext}}(\varphi, \psi) &:= \int_{\Omega_{\text{ext}}} \varphi(x)\, \psi(x)\, \det J_\sigma(x)\, \mathrm{d}x, \\
s^\sigma_{\text{ext}}(\varphi, \psi) &:= \int_{\Omega_{\text{ext}}} \big(J_\sigma(x)^{-T} \nabla\varphi(x)\big) \cdot \big(J_\sigma(x)^{-T} \nabla\psi(x)\big) \det J_\sigma(x)\, \mathrm{d}x, \\
r^\sigma(\psi) &:= \int_{\Omega_{\text{int}}} f\, \psi\, \mathrm{d}x.
\end{aligned}$$

We are now in a position to provide a precise formulation of the complex scaled Helmholtz problem [NW22, Section 2.3].

**Problem 5.3.** *Find $p \in H^1(\Omega)$, such that*

$$s_{int}(p, \hat{p}) + s^\sigma_{ext}(p, \hat{p}) - \omega^2 \left(m_{int}(p, \hat{p}) + m^\sigma_{ext}(p, \hat{p})\right) = r^\sigma(\hat{p})$$

*for all $\hat{p} \in H^1(\Omega)$.*

Since we are further interested in applying numerical methods to Problem 5.3, we begin by discretizing it in a suitable way.

## 5.2. Discrete formulation of the complex scaled Helmholtz problem

As usual, we start with picking a family of linearly independent functions,

$$\mathcal{B}_\mathcal{N} := \{b_0, \ldots, b_\mathcal{N}\} \subset H^1(\Omega),$$

and define the discrete space $\mathcal{X}_\mathcal{N}$ by

$$\mathcal{X}_\mathcal{N} := \operatorname{span}(\mathcal{B}_\mathcal{N}) \subset H^1(\Omega).$$

Furthermore we define mass- and stiffness matrices by

$$\mathbf{M} := (M_{i,j})_{i,j=0,\ldots,\mathcal{N}}, \qquad \mathbf{S} := (M_{i,j})_{i,j=0,\ldots,\mathcal{N}},$$

composed of the corresponding interior and exterior parts

$$M_{i,j} = m_{\text{int}}(b_i, b_j) + m^{\sigma}_{\text{ext}}(b_i, b_j),$$
$$S_{i,j} = s_{\text{int}}(b_i, b_j) + s^{\sigma}_{\text{ext}}(b_i, b_j).$$

Discretizing the right-hand side of 5.3, leads to,

$$\mathbf{r} := (r_i)_{i=0,\dots,\mathcal{N}},$$

with

$$r_i = r(b_i).$$

This allows us to formulate a discrete version of problem 5.3.

**Problem 5.4.** *Find $p \in \mathcal{X}_{\mathcal{N}}$, such that*

$$\mathbf{M}p - \omega^2 \mathbf{S}p = \mathbf{r}.$$

## 5.3. Interior Discretization

For the discretization of the interior domain $\Omega_{\text{int}}$, basically any discrete space

$$\mathcal{X}_{\text{int}} := \text{span}\{b_j, j = 0, \dots L\}, \tag{5.3}$$

is feasible, however, as we will see in chapter 5.4, we furthermore need the property that the trace space

$$\mathcal{X}_{\text{int}}|_{\Gamma} := \{tr_{\Gamma} f : f \in \mathcal{X}_{\text{int}}\} \subset H^1(\Gamma), \tag{5.4}$$

is an admissible finite subspace. This is required because we will use precisly this trace space as the finite element subspace of the surface space.

## 5.4. Exterior Discretization

In this section, we make use of the specific structure of the exterior domain to develop a simple discretization method that avoids the need of explicit meshing. As we have derived in Definition 5.1, we can identify the exterior domain $\Omega_{\text{ext}}$, via the mapping $\Psi$, with $R_{>0} \times \Gamma$.

Let

$$\mathcal{B}_N := \{\phi_n : n = 0, \dots, N\} \subset H^1(\mathbb{R}_{\geq 0}),$$
$$\mathcal{B}_M := \{\zeta_n : n = 0, \dots, N\} \subset H^1(\Gamma),$$

be families of linear independent functions. Based on these, we define discrete function spaces over $\mathbb{R}_{\geq 0}$ and $\Gamma$, by

$$\mathcal{X}^N_{\mathbb{R}} := \text{span}(\mathcal{B}_N) \subset H^1(\mathbb{R}_{\geq 0}), \qquad \mathcal{X}^M_{\Gamma} := \text{span}(\mathcal{B}_M) \subset H^1(\Gamma).$$

To discretize the exterior problem, we build a tensor product space of the form

$$\mathcal{X}^N_{\mathbb{R}} \otimes \mathcal{X}^M_{\Gamma} := \text{span}\left\{\phi \otimes \zeta : (\xi, \check{\mathbf{x}}) \mapsto \phi(\xi)\zeta(\check{\mathbf{x}}) \mid \phi \in \mathcal{B}_N,\ \zeta \in \mathcal{B}_M\right\}.$$

Note that a reasonable choice for the finite element subspace of $H^1(\Gamma)$ is given by, trace space of the interior space, $\mathcal{X}_{\text{int}}|_\Gamma$.

In order to assemble the entries of the mass and stiffness matrices we must evaluate the exterior bilinear forms for all combinations of basis functions. Since our basis functions are expressed as products of radial and tangential components, the bilinear form naturally decomposes into corresponding radial and tangential contributions (see, [NW22, Chapter 2 and 3] and [Wes20, Chapter 6]).

## 5.5. Coupling the interior and the exterior part

In our case, we will create a suitable finite element space by taking a truncated radial domain $(0, T)$ for some sufficiently large $T > 0$, pick the surface discretization of $\Gamma$, which is determined by the discretization of $\Omega_{\text{int}}$ and build the previously discussed product space. Lastly, we couple the interior and the exterior problem in a way, that the resulting basis functions are continuous on $\Omega$, with the aim of receiving a $H^1$-conform basis (for more detail, see [Wes20, Section 6.2.3]). This approach is reasonable, since we again expect exponentially decaying solutions and therefore assume that the truncation error decreases exponentially with respect to $T$.

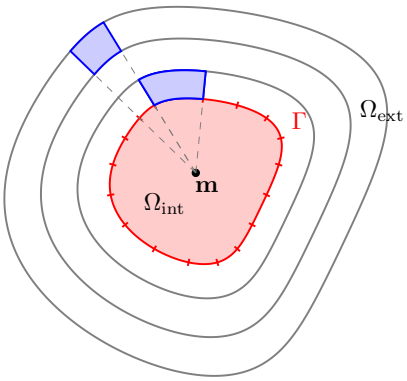


Figure 3.: Schematic representation of the exterior finite element product space for star-shaped domains.

In Figure 3, we present a schematic representation of the exterior product space. As presented, the surface discratization (illustrated in red), together with the radial discretization (illutstrated in grey) directly defines the resulting exterior product space mesh (illustrated in blue).

# 6. Implementation

From now on, our main objective lies in deriving a suitable set up for more generalized complex scalings and further providing numerical methods to model source problems on unbounded domains. Therefore we transform systems of the frequency domain, back into the time domain, to solve source problems in the time domain. First, we collect relevant information from previous chapters, to implement and test them.

## 6.1. Complex scalings into star-shaped coordinates

In this chapter we will present numerical tests of solving discrete source problem in the specific case of so called *star-shaped coordinates*. Defined as in 5.1, star-shaped coordinates describe the exterior domain by a surface coordinate and a radial coordinate with respect to some star shape point $\mathbf{m}$. In Figure 4 we present an example of star-shaped coordinates. As illustrated, $\mathbf{v}$ is defined by the star-shaped characteristics of $\Omega_{\text{int}}$.

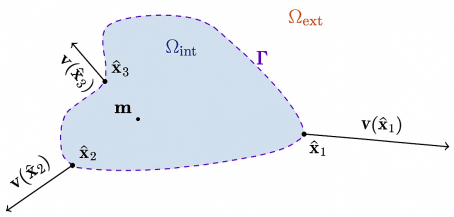


Figure 4.: An example of star-shaped coordinates in two dimensions [Wes20, Figure 7.2].

As derived in [Wes20, Section 7.2.2], the exterior part of the sesquilinear form for star-shape

coordinates is given by,

$$a^\sigma(\omega)(\varphi,\psi) := \frac{1}{\sigma(\omega)} \int_{\mathbb{R}_{>0}\times\Gamma} \frac{(1+\sigma(\omega)\,\xi)^2}{\mathbf{n}(\hat{\mathbf{x}})\cdot\mathbf{v}(\hat{\mathbf{x}})} \frac{\partial}{\partial\xi}\varphi(\xi,\hat{\mathbf{x}})\,\overline{\frac{\partial}{\partial\xi}\psi(\xi,\hat{\mathbf{x}})}\,d(\xi,\hat{\mathbf{x}}) \tag{6.1a}$$

$$- \frac{\sigma(\omega)}{4} \int_{\mathbb{R}_{>0}\times\Gamma} \frac{1}{\mathbf{n}(\hat{\mathbf{x}})\cdot\mathbf{v}(\hat{\mathbf{x}})} \varphi(\xi,\hat{\mathbf{x}})\,\overline{\psi(\xi,\hat{\mathbf{x}})}\,d(\xi,\hat{\mathbf{x}}) \tag{6.1b}$$

$$- \int_{\mathbb{R}_{>0}\times\Gamma} \frac{(1+\sigma(\omega)\,\xi)\,\mathbf{v}(\hat{\mathbf{x}})}{\mathbf{n}(\hat{\mathbf{x}})\cdot\mathbf{v}(\hat{\mathbf{x}})} \cdot \left(\widehat{\nabla}\varphi(\xi,\hat{\mathbf{x}})\right) \overline{\frac{\partial}{\partial\xi}\psi(\xi,\hat{\mathbf{x}})}\,d(\xi,\hat{\mathbf{x}}) \tag{6.1c}$$

$$- \int_{\mathbb{R}_{>0}\times\Gamma} \frac{(1+\sigma(\omega)\,\xi)\,\mathbf{v}(\hat{\mathbf{x}})}{\mathbf{n}(\hat{\mathbf{x}})\cdot\mathbf{v}(\hat{\mathbf{x}})} \left(\frac{\partial}{\partial\xi}\varphi(\xi,\hat{\mathbf{x}})\right) \cdot \overline{\widehat{\nabla}\psi(\xi,\hat{\mathbf{x}})}\,d(\xi,\hat{\mathbf{x}}) \tag{6.1d}$$

$$- \frac{\sigma(\omega)}{2} \int_{\mathbb{R}_{>0}\times\Gamma} \frac{\mathbf{v}(\hat{\mathbf{x}})}{\mathbf{n}(\hat{\mathbf{x}})\cdot\mathbf{v}(\hat{\mathbf{x}})} \cdot \widehat{\nabla}\left(\varphi(\xi,\hat{\mathbf{x}})\,\overline{\psi(\xi,\hat{\mathbf{x}})}\right) d(\xi,\hat{\mathbf{x}}) \tag{6.1e}$$

$$+ \sigma(\omega) \int_{\mathbb{R}_{>0}\times\Gamma} \frac{\|\mathbf{v}(\hat{\mathbf{x}})\|^2}{\mathbf{n}(\hat{\mathbf{x}})\cdot\mathbf{v}(\hat{\mathbf{x}})} \left(\widehat{\nabla}\varphi(\xi,\hat{\mathbf{x}})\right)^\top \cdot \overline{\widehat{\nabla}\psi(\xi,\hat{\mathbf{x}})}\,d(\xi,\hat{\mathbf{x}}) \tag{6.1f}$$

$$- \frac{1}{2} \int_\Gamma \frac{1}{\mathbf{n}(\hat{\mathbf{x}})\cdot\mathbf{v}(\hat{\mathbf{x}})} \mathrm{tr}_\Gamma\varphi(\hat{\mathbf{x}})\,\overline{\mathrm{tr}_\Gamma\psi(\hat{\mathbf{x}})}\,d\hat{\mathbf{x}} \tag{6.1g}$$

$$- \omega^2\sigma(\omega) \int_{\mathbb{R}_{>0}\times\Gamma} (1+\sigma(\omega)\,\xi)^2\,\mathbf{n}(\hat{\mathbf{x}})\cdot\mathbf{v}(\hat{\mathbf{x}})\,\varphi(\xi,\hat{\mathbf{x}})\,\overline{\psi(\xi,\hat{\mathbf{x}})}\,d(\xi,\hat{\mathbf{x}}). \tag{6.1h}$$

where $\widehat{\nabla}\varphi$ denotes the surface gradient, defined by,

$$\left(\widehat{\nabla}\varphi\right)\left(\varrho(\eta)\right) := \left(D\varrho(\eta)^\dagger\right)^\top \nabla_\eta(\varphi\circ\varrho)(\eta).$$

In the following sections we will focus on specific complex scalings of the form,

$$\sigma(\omega) := 1 + \frac{\alpha}{\gamma - i\omega} \qquad \in \mathbb{C}, \tag{6.2}$$

with $\alpha,\gamma\in\mathbb{R}$.

In addition, we will examine, how choosing $\alpha$ and $\gamma$ differently will influence the complex scaling and therefore the behavior of the solution.

## 6.2. Derivation of an adapted formulation

However, when inserting this specific choice of $\sigma$ into (6.1), some difficulties arise. As we aim to apply the Fourier transformation to the discrete Helmholtz problem 5.4, we want to make sure no rational dependencies of $-i\omega$ are contained, otherwise these terms result in convolution operators in time. However, (6.1f) for instance, will precisely lead to such an unwanted fraction. With the choice of $\sigma$ as in (6.2), (6.1f) takes the form as,

$$\begin{aligned} &+ \int_{\mathbb{R}_{>0}\times\Gamma} \frac{\|\mathbf{v}(\hat{\mathbf{x}})\|^2}{\mathbf{n}(\hat{\mathbf{x}})\cdot\mathbf{v}(\hat{\mathbf{x}})} \left(\widehat{\nabla}\varphi(\xi,\hat{\mathbf{x}})\right)^\top \cdot \overline{\widehat{\nabla}\psi(\xi,\hat{\mathbf{x}})}\,d(\xi,\hat{\mathbf{x}}) \\ &+ \frac{\alpha}{\gamma-i\omega} \int_{\mathbb{R}_{>0}\times\Gamma} \frac{\|\mathbf{v}(\hat{\mathbf{x}})\|^2}{\mathbf{n}(\hat{\mathbf{x}})\cdot\mathbf{v}(\hat{\mathbf{x}})} \left(\widehat{\nabla}\varphi(\xi,\hat{\mathbf{x}})\right)^\top \cdot \overline{\widehat{\nabla}\psi(\xi,\hat{\mathbf{x}})}\,d(\xi,\hat{\mathbf{x}}). \end{aligned} \tag{6.3}$$

Thus, we introduce an auxiliary function $h_1 \in H^1(\Omega_{\text{ext}})$ as,

$$h_1(\xi, \hat{x}) := \frac{\alpha}{\gamma + (-i\omega)} \varphi(\xi, \hat{x}),$$

such that (6.3), takes the form,

$$\begin{aligned} &+ \int_{\mathbb{R}_{>0} \times \Gamma} \frac{\|\mathbf{v}(\hat{\mathbf{x}})\|^2}{\mathbf{n}(\hat{\mathbf{x}}) \cdot \mathbf{v}(\hat{\mathbf{x}})} \left(\widehat{\nabla} \varphi(\xi, \hat{\mathbf{x}})\right)^\top \cdot \overline{\widehat{\nabla} \psi(\xi, \hat{\mathbf{x}})}\, d(\xi, \hat{\mathbf{x}}) \\ &+ \int_{\mathbb{R}_{>0} \times \Gamma} \frac{\|\mathbf{v}(\hat{\mathbf{x}})\|^2}{\mathbf{n}(\hat{\mathbf{x}}) \cdot \mathbf{v}(\hat{\mathbf{x}})} \left(\widehat{\nabla} h_1(\xi, \hat{\mathbf{x}})\right)^\top \cdot \overline{\widehat{\nabla} \psi(\xi, \hat{\mathbf{x}})}\, d(\xi, \hat{\mathbf{x}}). \end{aligned} \tag{6.4}$$

Altogether, six auxiliary functions are needed to eliminate all undesired fractions of $-i\omega$ and to reduce the order in $-i\omega$.

To be precise we define,

$$\begin{aligned} h_1(\xi, \hat{x}) &:= \frac{\alpha}{\gamma + (-i\omega)} \varphi(\xi, \hat{x}), \\ h_2(\xi, \hat{x}) &:= -i\omega\, h_1(\xi, \hat{x}), \\ h_3(\xi, \hat{x}) &:= \frac{\alpha}{\gamma + (-i\omega)} h_2(\xi, \hat{x}), \\ h_4(\xi, \hat{x}) &:= \frac{\alpha}{\gamma + (-i\omega)} \varphi(\xi, \hat{x}), \\ h_5(\xi, \hat{x}) &:= -i\omega\, \varphi, \\ h_6(\xi, \hat{x}) &:= \frac{\alpha}{\alpha + \gamma + (-i\omega)} \varphi, \end{aligned} \tag{6.5}$$

such that the adapted bilinearforms $\tilde{m}^\sigma_{\text{ext}}$ and $\tilde{s}^\sigma_{\text{ext}}$ now additionally depend on these auxiliary functions, as shown in A.5. This allows us to introduce the following formulation of the first-order complex-scaled Helmholtz equation into star-shaped coordinates.

**Problem 6.1.** *Find* $p, q \in H^1(\Omega_{\text{int}}), \mathbf{g} \in H^1(\Omega_{\text{ext}})^6$, *such that*

$$\begin{aligned} s_{\text{int}}(p, \hat{p}, \mathbf{g}, \mathbf{h}) - m_{\text{int}}(q, \hat{q}, \mathbf{g}, \mathbf{h}) + \tilde{m}^\sigma_{\text{ext}}(p, \hat{p}, \mathbf{g}, \mathbf{h}) + \\ + (-i\omega) \left[\tilde{s}^\sigma_{\text{ext}}(p, \hat{p}, \mathbf{g}, \mathbf{h}) + m_{\text{int}}(q, \hat{p}, \mathbf{g}, \mathbf{h}) + m_{\text{int}}(p, \hat{q}, \mathbf{g}, \mathbf{h})\right] = r(\hat{p}) \end{aligned} \tag{6.6}$$

*for all* $\hat{p}, \hat{q} \in H^1(\Omega_{\text{int}}), \mathbf{h} \in H^1(\Omega_{\text{ext}})^6$.

With,

$$\begin{aligned} m_{\text{int}}(\varphi, \psi, \mathbf{g}, \mathbf{h}) &:= \int_{\Omega_{\text{int}}} \varphi(x)\, \psi(x)\, \mathrm{d}x, \\ s_{\text{int}}(\varphi, \psi, \mathbf{g}, \mathbf{h}) &:= \int_{\Omega_{\text{int}}} \nabla \varphi(x) \cdot \nabla \psi(x)\, \mathrm{d}x, \\ r(\psi) &:= \int_{\Omega_{\text{int}}} f\, \psi\, \mathrm{d}x, \end{aligned}$$

and $\tilde{m}^\sigma_{\text{ext}}, \tilde{s}^\sigma_{\text{ext}}$ as in A.5.

In the following, we construct the interior and exterior finite element spaces, as previously outlined in Chapter 5. Applying this discretization to Problem 6.1 results in the following formulation.

**Problem 6.2.** *Find* $\mathbf{p}$ *such that*

$$-i\omega\mathcal{M}\mathbf{p} + \mathcal{S}\mathbf{p} = \mathbf{r}. \tag{6.7}$$

In the continuous problem formulation 6.1, the bilinearforms depend on auxiliary functions, represented by $\mathbf{h}$ and $\mathbf{g}$, in addition to the primary variables $p, \hat{p}$ and $q, \hat{q}$. These auxiliary functions arise from preparation and reductions of the system, to obtain a formulation that is amenable to the Fourier transformation and results in a well posed system in the time domain.

As presented in A.5, $\mathbf{h}$ is known to contain only scalar multiples of the primary functions p and q. Thus, we chose to omit their explicit appearance in the discrete problem formulation 6.2. We combined the primary and auxiliary functions into the vector $\mathbf{p}$ so that its dimension matches those of the system matrices $\mathcal{M}$ and $\mathcal{S}$. Furthermore, $\mathbf{r}$ denotes the corresponding right hand side. Compared to Problem 5.4, this formulation leads to an increased system size due to the implicit inclusion of the auxiliary functions.

## 6.3. Solving the time-domain source problem

So far, we have prepared the necessary framework to introduce a well posed time-domain formulation to solve the source problem. Now we only need to transform Problem 6.2 into the time-domain, by applying the inverse Fourier transformation. Thanks to introducing the auxiliary functions, the transformed time-domain problem is well-posed.

**Problem 6.3.** *Find* $\mathbf{p}$ *such that*

$$\mathcal{M}\dot{\mathbf{p}} + \mathcal{S}\mathbf{p} = \mathbf{r}. \tag{6.8}$$

In order to pose a coherent discrete problem formulation for the wave equation, one has to equip problem 6.3 with a suitable initial condition $\mathbf{p_0}$, representing the initial state. This condition must be chosen carefully, since only a subset of the entries of $\mathbf{p}$ corresponds to the solution within the interior domain $\Omega_{\text{int}}$. Since the functions in 6.5 are defined only in the frequency domain, we need to equip them with homogeneous initial conditions at $t = 0$, to ensure well-posedness of the problem in the time domain. Similarly to section 4.3, we do not distinguish between the symbol of the functions in the frequency domain and the time domain.

Assume, similarly to (2.2), $p_0$ and $p_1$ represent the initial state and acceleration of the wave in the interior domain, and $\mathbf{p_0}$ represents these in the format of problem 6.3. Then the equations to be solved can be formulated as,

$$\begin{aligned} \mathcal{M}\dot{\mathbf{p}}(t) + \mathcal{S}\mathbf{p}(t) &= \mathbf{r}(t), \\ \mathbf{p}(t_0) &= \mathbf{p_0}. \end{aligned} \tag{6.9}$$

Note that system (6.9) only depends on a single variable $\mathbf{p}$. This is because we have combined the functions from Problem 6.1 into a single vector, with the internal couplings

between these functions fully represented. As a result, the interactions that would normally appear as separate terms are already incorporated into the assembled matrices, allowing the system to be expressed solely in terms of $\mathbf{p}$. As already briefly discussed in section 2.1 one common way of solving (6.9) is to apply the Crank-Nicolson method. However, in contrast to Algorithm A, the following version of the Crank-Nicolson method reduced to solving only one equation.

**Algorithm B (Crank–Nicolson in one variable).**
*At each time step with step size $\tau > 0$:*
*Solve:*

$$\mathcal{M}\left(\frac{\mathbf{p}^{n+1} - \mathbf{p}^n}{\tau}\right) + \mathcal{S}\left(\frac{\mathbf{p}^{n+1} + \mathbf{p}^n}{2}\right) = \frac{\mathbf{r}^{n+1} + \mathbf{r}^n}{2}$$

Recalling that $p$ denotes the wave in the interior domain $\Omega_{\text{int}}$. According to [Jün23, Section 7.3], the wave equation system preserves energy when the right hand side $f = 0$. To be precise, the energy defined by,

$$E(t) = \int_{\Omega} (\partial_t p(x,t)^2 + |\nabla p(x,t)|^2)\, dx, \tag{6.10}$$

remains constant in time. Furthermore the Crank-Nicolson method preserves this quantity, even in the discretized framework, (see, e.g. [MF24, Section 3.2.3]).

# 7. Numerical tests and results

In the following, we will numerically investigate the behavior of the solution that our method yields. We will see how our method provides stable solutions in standard settings. However, since previous studies have reported instabilities in more challenging configurations, we further examine the robustness and applicability of our method. We show that appropriate parameter tuning ensures stable solutions in all tested settings.

## 7.1. First results

We begin by solving (6.9) on a squared domain, using a point source as the initial condition $p_0$ and a homogeneous right-hand side. All model parameters are summarized in Table 2.

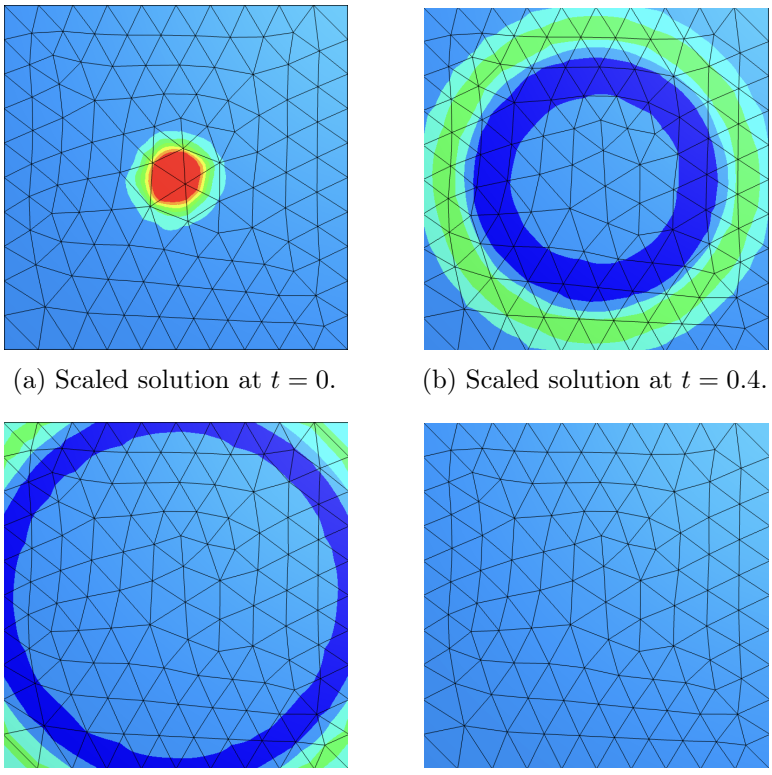

(a) Scaled solution at $t = 0$.

(b) Scaled solution at $t = 0.4$.

(c) Scaled solution at $t = 0.6$.

(d) Scaled solution at $t = 4$.

Figure 5.: Solution of the complex-scaled wave equation (6.9) for various times $t$ in $\Omega_{\text{int}}$. The color bar ranges from $-0.05$ (dark blue) to 0 (light blue) to 0.2 (red).

Figure 5 illustrates the evolution of the solution to (6.9) at various times t in $\Omega_{\text{int}}$. Image

5a shows the initial state $p_0$, while Figures 5b and 5c illustrate the propagation of the scaled solution. In particular, Figure 5c provides a clear demonstration of how the wave energy exits $\Omega_{\text{int}}$. In 5d we see that the damping ensures that no artifacts occur.

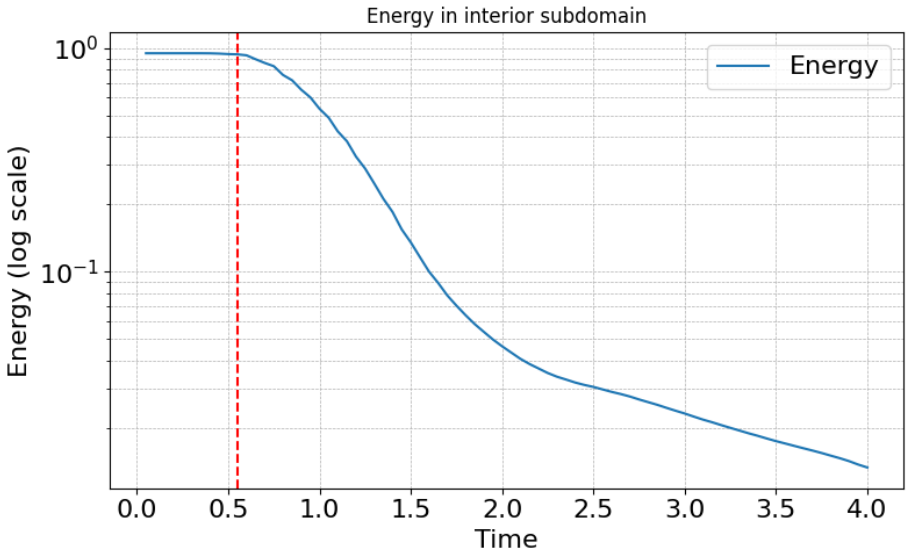


Figure 6.: Energy of solution in $\Omega_{\text{int}}$.

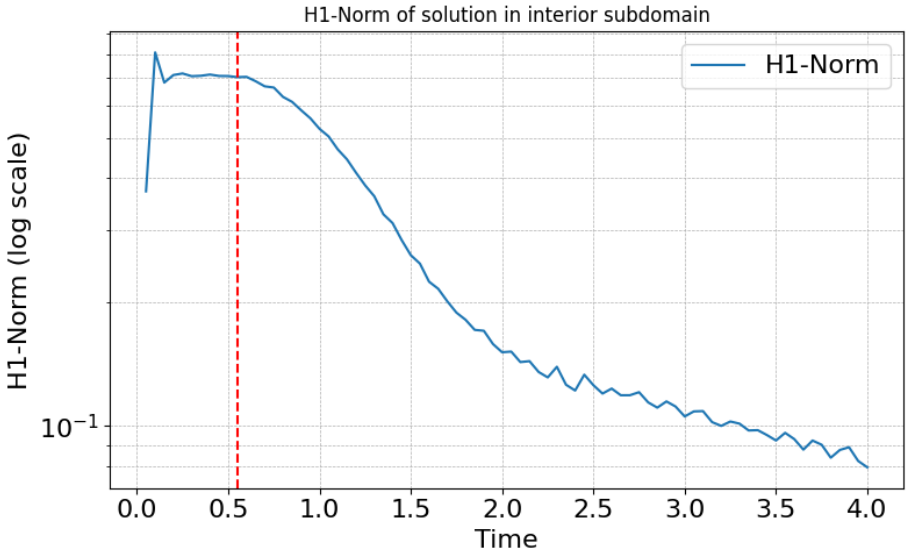


Figure 7.: $H^1$-Norm of solution in $\Omega_{\text{int}}$.

Figure 6 illustrates the decay of the energy of the scaled solution, as defined in (6.10). As long as the wave peak remains entirely within the interior domain, the energy is conserved. Once the wave enters the exterior domain, however, the energy decreases, since the damping

in $\Omega_{\text{ext}}$ is designed to produce precisely this effect. Figure 7 illustrates that the solution remains damped, with almost no reflections returning to the interior domain. The red dotted line indicates approximately the time at which the wave peak first reaches the boundary $\Gamma$.

We are furthermore interested in how the scaled solution exhibits in the interior domain in comparison to an unscaled reference solution. We expect that the error[1] between the scaled and the reference solution decreases as the mesh is refined. Naturally, this comparison is only meaningful up to the point where the wave propagates through $\Gamma$. All model parameters are summarized in Table 4.

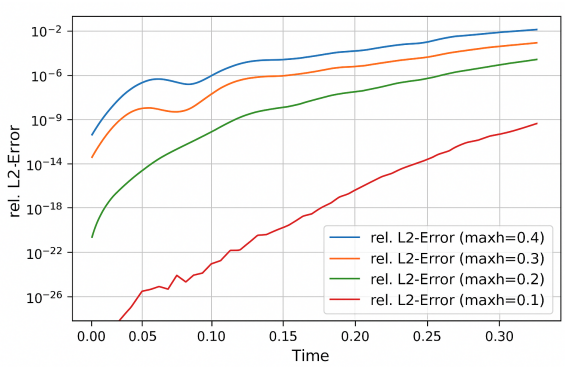


Figure 8.: Relative $L^2$–error between the scaled and reference solutions for different mesh sizes.

Figure 9 shows the temporal evolution of the energy (6.10) in the interior domain for the scaled and unscaled solutions. Compared to the scaled solution, the unscaled solution reflects at the boundary of $\Omega_{\text{ext}}$, which leads to an increase in energy at later times. All model parameters are summarized in Table 5.

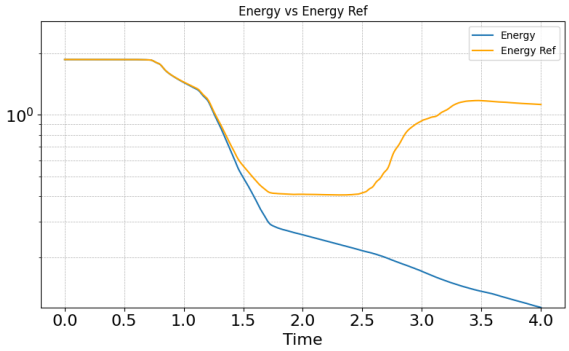


Figure 9.: Energy of scaled and unscaled solution in $\Omega_{\text{int}}$.

[1] defined as $\frac{\|p_{ref}-p\|_{L2}^2}{\|p_{ref}\|_{L2}^2}$

## 7.2. Observation of Instabilities

In [RSS12] Ruprecht et. al present the pole condition approach for transparent boundary conditions for time-dependent, two dimensional problems, aiming to suppress physically unmeaningful modes when solving PDEs on open domains. While the method performs well for the application on Schrödinger and drift-diffusion equations, it exhibits numerical instabilities for wave-type equations. As presented in [NW22], the approach from [RSS12] is equivalent to our complex scaling method, however, different basis functions for the finite element space were used. We try to explain the cause of this instability and will take a closer look at the underlying eigenvalues.

As shown in [RSS12, Figure 4.10], their method unexpectedly yielded poorer results when using higher-order discretizations.

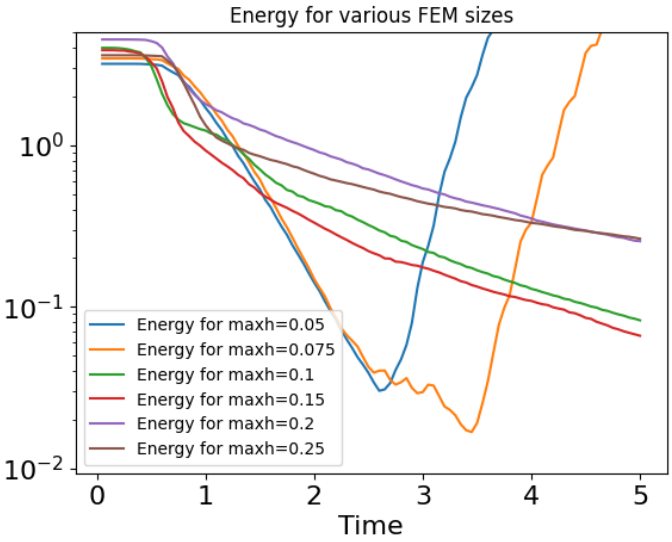


Figure 10.: Recreation of instability from [RSS12]. Energy defined as in 6.10, for various FEM sizes.

Figure 10 reflects the results of [RSS12] within our specific setting, where the energy is again defined as in 6.10. However, in order to recreate a framework that resembles this instability, we had to choose very specific settings (see, Table 6). Within our formulation, the method described in [RSS12] can be recovered by choosing $\gamma = 0$. In the following we explain this behavior by examining the underlying eigenvalues of the system.

### 7.2.1. Stability Analysis

We have already see in Section (7.1) that our method produces reasonable solutions. In particular, the solutions exhibit a natural wave-like behavior within $\Omega_{\text{int}}$ and are damped outside the domain of interest, thereby preventing unphysical reflections. However, in the setting of Figure 10 we have seen that numerical instabilities occurred. Therefore we want to provide a general reasoning how parameter choices influence the stability of the solution

to 6.9, even for larger time scales. Rather than directly investigating the behavior of the solution itself, we can analyze the eigenvalues of the frequency-domain system matrices in Problem 6.2, because they give insight on the stability of the solution. Eigenvalues provide direct information about the stability properties of the system and allow one to infer the qualitative behavior of the solution without performing long time computations.

### Stability Analysis via Eigenvalues

We begin by recalling the homogeneous Helmholtz problem,

$$-\Delta u(\mathbf{x}) - \omega^2 u(\mathbf{x}) = 0. \tag{7.1}$$

If, for a given frequency $\omega$, there exists a non trivial function $u_\omega$ that solves (7.1), we call $\omega$ eigenfrequency with respective eigenfunction $u_\omega$. Assuming that there exists a complete system of orthonormal eigenfunction $u_{\omega_n}, n \in \mathbb{N}_0$ of the operator $-\Delta$ with suitable boundary conditions, then the solution of (7.1) can be decomposed into,

$$u(\mathbf{x}) = \sum_{n=0}^{\infty} \frac{(f, u_{\omega_n})}{\omega_n^2 - \omega^2} u_{\omega_n}(\mathbf{x}). \tag{7.2}$$

[Wes20, Section 1.1]

As the inverse Fourier transformation yields exponential factors $e^{-i\omega_n t}$, the imaginary parts of the eigenfrequencies determine the asymptotic behavior of the time-domain solution [Obe90, Section 1.3]. The same theory can be applied in the discretized framework. However, in this case the decomposition into basis function is guaranteed since the solution belongs to the finite element space. Therefore we can investigate stability of the time domain solution by computing the eigenvalues of,

$$-i\omega\mathcal{M}\mathbf{p} + \mathcal{S}\mathbf{p} = 0. \tag{7.3}$$

In the following we investigate the eigenvalues of (7.3) for different finite element approximations.

According to [Wes20, Section 5.4], the *essential spectrum* consists of all frequencies $\omega$ that satisfy

$$\arg(\sigma(\omega)) \in [\pi - \mu, \pi + \mu], \tag{7.4}$$

as well as the frequencies that lie on the explicitly defined curve

$$\Re\left(-i\omega\left(1 + \frac{\alpha}{\gamma - i\omega}\right)\right) = 0, \tag{7.5}$$

where $\mu$ is determined by the radial component $\mathbf{v}$ and the geometry of $\Omega_{\text{int}}$. This suggests that in our framework the star-shape center $\mathbf{m}$, as well as the parameters $\alpha$ and $\gamma$ determine the location of the eigenfrequencies in the complex plane. For more detail regarding the *essential spectrum* we refer to [Wes20, Section 5].

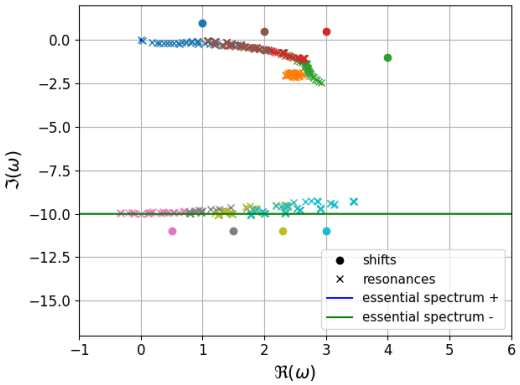


(a) Resonances for $\gamma = 0, \mathbf{m} = (0, 0)$.

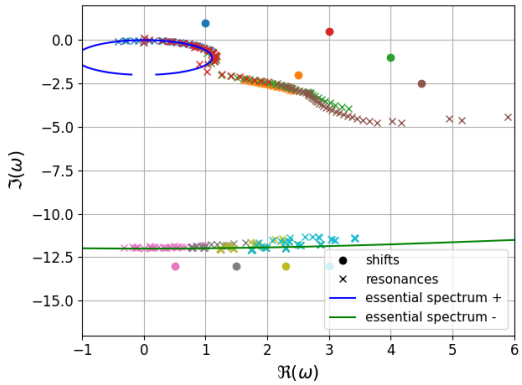


(b) Resonances for $\gamma = 2.0, \mathbf{m} = (0, 0)$.

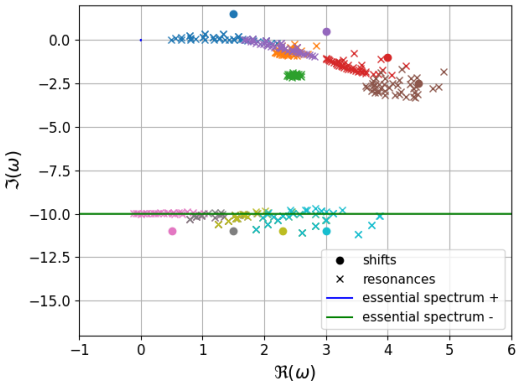


(c) Resonances for $\gamma = 0, \mathbf{m} = (0.45, 0.45)$.

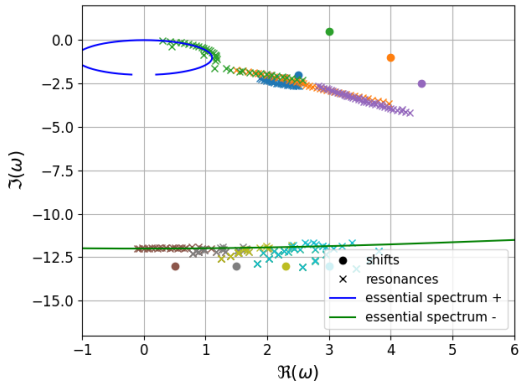


(d) Resonances for $\gamma = 2.0, \mathbf{m} = (0.45, 0.45)$.

Figure 11.: Comparison of computed resonances for different parameters.

Figure 11 illustrates how different choices of $\gamma$ and $\mathbf{m}$ determine the location of the essential spectrum in the complex plane. The resonances on the blue and green lines correspond to those defined by (7.5), while the others belong to (7.4). Figure 11a shows the configuration for a favorable star-shaped center $\mathbf{m}$ and $\gamma = 0$. Because $\gamma = 0$, the positive and negative branches of (7.5) align. Overall, all resolved frequencies have a non-positive imaginary part, ensuring stability in the time domain. When a positive $\gamma$ is introduced, as shown in Figure 11b, the curve from (7.5) splits. More importantly, the introduction of $\gamma$ shifts the resonances corresponding to (7.4) downwards in the complex plane. In contrast, the less favorable configuration shown in Figure 11c reveals eigenfrequencies with strictly positive imaginary parts. Precisely this scenario occurred in the setting of Figure 10. The unintuitive behavior, where a higher FEM resolution leads to poorer results, can be explained as follows. The unfavorable geometric configuration caused the appearance of eigenfrequencies with positive imaginary parts, which are responsible for the system's instability in the time domain. While sufficiently fine discretizations resolve a wider range of these unstable frequencies, low-quality discretizations leave many of them unresolved. Consequently, a low-order FEM discretization gives the impression of a stable method, even though this stability is merely apparent. By introducing a $\gamma > 0$, the part of the essential spectrum with positive imaginary parts can

be shifted into the lower half-plane, leading to numerically stable solutions in the time domain. Throughout all tests investigating resonances, we followed a shift-and-invert Arnoldi approach for resolving desired eigenfrequencies. All model parameters are summarized in Table 7.

## 7.3. Further results through stability improvements

In the previous sections, we have observed that certain instabilities may arise under unfavorable conditions. With the knowledge gained from the previous section, we now aim to identify special parameter settings, enabled by our specific definition of $\sigma$ (see, 6.2), that guarantee robustness. Following the approach in [HKW24, Section 5], we attempt to adjust parameters to shift the spectrum toward favorable regions.

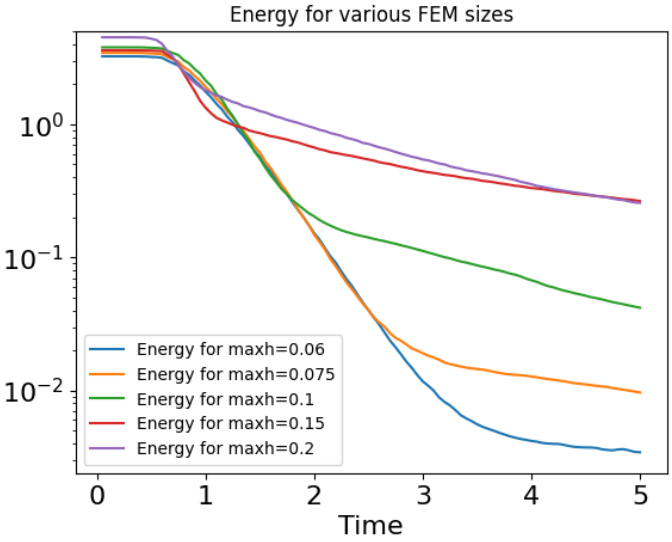


Figure 12.: Robustness of our method for several mesh sizes, (see, Table 8).

Even in the unfavorable case that led to unstable solutions shown in Figure 10, our method guarantees robustness. By replacing $\gamma = 0$ with $\gamma = 2.0$, our method yields stable solutions. As illustrated in Figure 12, increasing the degrees of freedom of the finite element space does not lead to any instabilities. The additional flexibility introduced through the parameter $\gamma$ further enhances robustness. As shown in Figure 11, $\gamma$ effectively shifts the essential spectrum in the complex plane. By tuning $\gamma$, it becomes possible to shift the spectrum into the negative imaginary domain, thereby ensuring stability. We have now achieved the desired state, in which increasing the discretization quality not only ensures that the solution remains damped in $\Omega_{\text{ext}}$, but also causes the energy in $\Omega_{\text{int}}$ to decay even faster.

# 8. Conclusion and Outlook

In this thesis, we first examined existing Perfectly Matched Layer methods and approaches for solving source problems in open systems, with particular attention to how parameter tuning influences the quality of the solutions. Building on this foundation, we introduced a more general framework based on the findings of [Wes20]. Using these results, we derived a method for solving source problems on star-shaped domains that yields numerically stable solutions. Furthermore, we applied our method to the framework studied in [RSS12], where their approach had failed for wave-type equations, and provided a theoretical explanation for the reasons behind this failure. Our results demonstrated that the proposed method successfully resolves these issues and produces stable and accurate solutions. Finally, we offered practical guidance on parameter tuning to ensure robustness across different geometries and configurations.

Open questions remain concerning a detailed analysis of the essential spectrum—specifically, how the interplay between geometry and the radial scaling component determines its location in the complex plane, especially for more advanced geometries. It also remains to be investigated whether, even for favorable choices of star-shaped center points (such as those located at the geometric center), higher spatial resolution might lead to eigenfrequencies with positive imaginary parts (with $\gamma = 0$, in our specific choice of $\sigma$), and thus to unstable solutions in the time domain.

# A. Appendix

## A.1. The Fourier transformation

We start by introducing the (inverse) Fourier transform.

**Definition A.1.** *Let $f \in L^1(\mathbb{R}^n)$. We define the* Fourier transform *of $f$ by:*

$$\hat{f}(y) := \frac{1}{(2\pi)^{n/2}} \int_{\mathbb{R}^n} e^{-ix\cdot y} f(x)\, dx \quad (y \in \mathbb{R}^n)$$

*The* inverse Fourier transform *is given by:*

$$\check{f}(y) := \frac{1}{(2\pi)^{n/2}} \int_{\mathbb{R}^n} e^{ix\cdot y} f(x)\, dx \quad (y \in \mathbb{R}^n)$$

As proven in [Eva10, Section 4.3.1], the (inverse) Fourier transform fulfills some important properties.

**Theorem A.2** (Properties of Fourier transform)**.** *Assume $f \in L_2(\mathbb{R})$, then:*

$$\widehat{D^\alpha f} = (iy)^\alpha \hat{f} \quad \text{for each multiindex } \alpha \text{ such that } D^\alpha f \in L^2(\mathbb{R}^n),$$
$$f = \check{\hat{f}}$$

## A.2. Preliminaries

In the following let $\Omega_{\text{int}}, \Omega_{\text{ext}}, \Omega, \Gamma \subset \mathbb{R}^2$. Moreover, we assume that these sets fulfill the following assumptions:

(B1) $\Omega_{\text{int}}, \Omega_{\text{ext}}, \Omega, \neq \emptyset$ are open domains and $\Gamma$ is a 1-dimensional manifolds,

(B2) the sets $\Omega_{\text{int}}, \Gamma$ and $\Omega_{\text{ext}}$ are pairwise disjoint

$$\Omega_{\text{int}} \cup \Gamma \cup \Omega_{\text{ext}} = \Omega, \quad \text{and} \quad \Gamma = \partial\Omega_{\text{int}},$$

(B3) $\Omega_{\text{int}}$ is bounded and

(B4) $\partial\Omega, \Gamma$ are locally Lipschitz.

## A.3. Model parameters for various numerical tests

| Parameter | Value | Notes |
|---|---|---|
| $\omega$ | 10 | frequency |
| $\alpha$ | 1 | PML parameter |
| $\mathrm{p}_0$ | $\exp\left(-4^2\left((x-0.2)^2+(y-0.2)^2\right)\right)$ | initial condition |
| $\mathrm{p}_1$ | 0 | initial condition |
| f | 0 | right-hand side |
| maxh | 0.2 | max. mesh size |
| order | 4 | order of FE-space basis polynomials |
| $\Omega_{\text{int}}$ | $[0,2]^2$ | interior domain |
| $\Omega_{\text{ext}}$ | $[0,4]^2 \setminus \Omega_{\text{int}}$ | exterior domain |

Table 1.: Problem setup and model parameters for the Cartesian-scaled Helmholtz equation.

| Parameter | Value | Notes |
|---|---|---|
| $\alpha$ | 20.0 | scaling parameter |
| $\gamma$ | 2.0 | scaling parameter |
| $\mathrm{p}_0$ | $\frac{1}{2}\exp\left(-2\cdot 20^2\left(x^2+y^2\right)\right)$ | initial condition |
| $\mathrm{p}_1$ | 0 | initial condition |
| $\tau$ | 0.01 | time-step size |
| $\mathcal{T}_{\text{end}}$ | 4.0 | end time f |
| 0 | right-hand side | |
| T | 1 | length of truncated radial dimension |
| maxh | 0.1 | max. mesh size $\Omega_{\text{int}}$ |
| maxh_1d | 0.1 | max. mesh size of $\mathcal{X}_T \subset H^1(0,T)$ |
| order | 3 | order of FE-space $\mathcal{X}_{\text{int}} \subset H^1(\Omega_{\text{int}})$ |
| order_1d | 3 | order of FE-space $\mathcal{X}_\Gamma \subset H^1(\Omega_\Gamma)$ |
| $\Omega_{\text{int}}$ | $[0,1]^2$ | interior domain |
| $\mathbf{m}$ | (0,0) | star shape point |

Table 2.: Problem setup and model parameters for the complex scaled wave equation.

| Parameter | Value | Notes |
|---|---|---|
| $\alpha$ | 20.0 | scaling parameter |
| T | 1 | length of truncated radial dimension |
| maxh | 0.1 | max. mesh size $\Omega_{\text{int}}$ |
| maxh_1d | 0.1 | max. mesh size of $\mathcal{X}_T \subset H^1(0,T)$ |
| order | 3 | order of FE-space $\mathcal{X}_{\text{int}} \subset H^1(\Omega_{\text{int}})$ |
| order_1d | 3 | order of FE-space $\mathcal{X}_\Gamma \subset H^1(\Omega_\Gamma)$ |
| $\Omega_{\text{int}}$ | $[0,1]^2$ | interior domain |
| **m** | (-0.3,-0.2) | star shape point |

Table 3.: Problem setup and model parameters for the eigenvalue problem.

| Parameter | Value | Notes |
|---|---|---|
| $\alpha$ | 20.0 | scaling parameter |
| $\gamma$ | 2.0 | scaling parameter |
| $\mathrm{p}_0$ | $\exp\left(-20^2\left(x^2+y^2\right)\right)$ | initial condition |
| $\mathrm{p}_1$ | 0 | initial condition |
| T | 1 | length of truncated radial dimension |
| $\tau$ | 0.01 | time-step size |
| $\mathcal{T}_{\text{end}}$ | 4.0 | end time |
| order | 3 | order of FE-space $\mathcal{X}_{\text{int}} \subset H^1(\Omega_{\text{int}})$ |
| order_1d | 3 | order of FE-space $\mathcal{X}_\Gamma \subset H^1(\Omega_\Gamma)$ |
| $\Omega_{\text{int}}$ | $[0,1]^2$ | interior domain |
| **m** | (0.3,0.3) | star shape point |

Table 4.: Problem setup and model parameters for convergence investigation.

| Parameter | Value | Notes |
|---|---|---|
| $\alpha$ | 20.0 | scaling parameter |
| $\gamma$ | 2.0 | scaling parameter |
| $\mathrm{p}_0$ | $\exp\left(-20^2\left((x+0.2)^2+(y+0.2)^2\right)\right)$ | initial condition |
| $\mathrm{p}_1$ | 0 | initial condition |
| T | 1 | length of truncated radial dimension |
| $\tau$ | 0.01 | time-step size |
| $\mathcal{T}_{\text{end}}$ | 4.0 | end time |
| maxh | 0.1 | max. mesh size $\Omega_{\text{int}}$ |
| maxh_1d | 0.1 | max. mesh size of $\mathcal{X}_T \subset H^1(0,T)$ |
| order | 3 | order of FE-space $\mathcal{X}_{\text{int}} \subset H^1(\Omega_{\text{int}})$ |
| order_1d | 3 | order of FE-space $\mathcal{X}_\Gamma \subset H^1(\Omega_\Gamma)$ |
| $\Omega_{\text{int}}$ | $[0,1]^2$ | interior domain |
| **m** | (0.2,-0.2) | star shape point |

Table 5.: Problem setup and model parameters for energy investigation.

| Parameter | Value | Notes |
|---|---|---|
| $\alpha$ | 20.0 | scaling parameter |
| $\gamma$ | 0.0 | scaling parameter |
| $p_0$ | $\exp\left(-20^2\left(x^2+y^2\right)\right)$ | initial condition |
| $p_1$ | 0 | initial condition |
| T | 1 | length of truncated radial dimension |
| $\tau$ | 0.05 | time-step size |
| $\mathcal{T}_{\text{end}}$ | 5.0 | end time |
| maxh | 0.1 | max. mesh size $\Omega_{\text{int}}$ |
| maxh_1d | 0.1 | max. mesh size of $\mathcal{X}_T \subset H^1(0,T)$ |
| order | 3 | order of FE-space $\mathcal{X}_{\text{int}} \subset H^1(\Omega_{\text{int}})$ |
| order_1d | 2 | order of FE-space $\mathcal{X}_\Gamma \subset H^1(\Omega_\Gamma)$ |
| $\Omega_{\text{int}}$ | $[0,1]^2$ | interior domain |
| $\mathbf{m}$ | (0.35,0.35) | star shape point |

Table 6.: Problem setup and model parameters for recreation of result of [RSS12].

| Parameter | Value | Notes |
|---|---|---|
| $\alpha$ | 10.0 | scaling parameter |
| T | 1.5 | length of truncated radial dimension |
| maxh | 0.1 | max. mesh size $\Omega_{\text{int}}$ |
| maxh_1d | 0.01 | max. mesh size of $\mathcal{X}_T \subset H^1(0,T)$ |
| order | 2 | order of FE-space $\mathcal{X}_{\text{int}} \subset H^1(\Omega_{\text{int}})$ |
| order_1d | 2 | order of FE-space $\mathcal{X}_\Gamma \subset H^1(\Omega_\Gamma)$ |
| $\Omega_{\text{int}}$ | $[0,1]^2$ | interior domain |

Table 7.: Problem setup and model parameters for eigenvalues investigation

| Parameter | Value | Notes |
|---|---|---|
| $\alpha$ | 20.0 | scaling parameter |
| $\gamma$ | 2.0 | scaling parameter |
| $\mathrm{p}_0$ | $\exp\left(-20^2\left(x^2+y^2\right)\right)$ | initial condition |
| $\mathrm{p}_1$ | 0 | initial condition |
| T | 1 | length of truncated radial dimension |
| $\tau$ | 0.05 | time-step size |
| $\mathcal{T}_{\text{end}}$ | 5.0 | end time |
| order | 3 | order of FE-space $\mathcal{X}_{\text{int}} \subset H^1(\Omega_{\text{int}})$ |
| order_1d | 2 | order of FE-space $\mathcal{X}_\Gamma \subset H^1(\Omega_\Gamma)$ |
| $\Omega_{\text{int}}$ | $[0,1]^2$ | interior domain |
| $\mathbf{m}$ | (0.35,0.35) | star shape point |

Table 8.: Problem setup and model parameters for test of robustness.

## A.4. Exterior part of complex scaled sesquilinearform into star shaped coordinates

$$
\begin{aligned}
a^{\sigma}_{\mathrm{ext}}(\omega)(\varphi,\psi) := & \int_{\mathbb{R}_{>0}\times\Gamma} \frac{1}{\mathbf{n}(\hat{\mathbf{x}})\cdot\mathbf{v}(\hat{\mathbf{x}})}\frac{\partial}{\partial\xi}\varphi(\xi,\hat{\mathbf{x}})\overline{\frac{\partial}{\partial\xi}\psi(\xi,\hat{\mathbf{x}})}\,d(\xi,\hat{\mathbf{x}}) && \text{(A.1a)}\\
& - \frac{\alpha}{\gamma-i\omega+\alpha}\int_{\mathbb{R}_{>0}\times\Gamma} \frac{1}{\mathbf{n}(\hat{\mathbf{x}})\cdot\mathbf{v}(\hat{\mathbf{x}})}\frac{\partial}{\partial\xi}\varphi(\xi,\hat{\mathbf{x}})\overline{\frac{\partial}{\partial\xi}\psi(\xi,\hat{\mathbf{x}})}\,d(\xi,\hat{\mathbf{x}}) && \text{(A.1b)}\\
& + \int_{\mathbb{R}_{>0}\times\Gamma} \frac{2\xi+\xi^2}{\mathbf{n}(\hat{\mathbf{x}})\cdot\mathbf{v}(\hat{\mathbf{x}})}\frac{\partial}{\partial\xi}\varphi(\xi,\hat{\mathbf{x}})\overline{\frac{\partial}{\partial\xi}\psi(\xi,\hat{\mathbf{x}})}\,d(\xi,\hat{\mathbf{x}}) && \text{(A.1c)}\\
& + \frac{\alpha}{\gamma-i\omega}\int_{\mathbb{R}_{>0}\times\Gamma} \frac{\xi^2}{\mathbf{n}(\hat{\mathbf{x}})\cdot\mathbf{v}(\hat{\mathbf{x}})}\frac{\partial}{\partial\xi}\varphi(\xi,\hat{\mathbf{x}})\overline{\frac{\partial}{\partial\xi}\psi(\xi,\hat{\mathbf{x}})}\,d(\xi,\hat{\mathbf{x}}) && \text{(A.1d)}\\
& - \frac{1}{4}\int_{\mathbb{R}_{>0}\times\Gamma} \frac{1}{\mathbf{n}(\hat{\mathbf{x}})\cdot\mathbf{v}(\hat{\mathbf{x}})}\varphi(\xi,\hat{\mathbf{x}})\,\overline{\psi(\xi,\hat{\mathbf{x}})}\,d(\xi,\hat{\mathbf{x}}) && \text{(A.1e)}\\
& - \frac{1}{4}\frac{\alpha}{\gamma-i\omega}\int_{\mathbb{R}_{>0}\times\Gamma} \frac{1}{\mathbf{n}(\hat{\mathbf{x}})\cdot\mathbf{v}(\hat{\mathbf{x}})}\varphi(\xi,\hat{\mathbf{x}})\,\overline{\psi(\xi,\hat{\mathbf{x}})}\,d(\xi,\hat{\mathbf{x}}) && \text{(A.1f)}\\
& - \int_{\mathbb{R}_{>0}\times\Gamma} \frac{(1+\xi)\mathbf{v}(\hat{\mathbf{x}})}{\mathbf{n}(\hat{\mathbf{x}})\cdot\mathbf{v}(\hat{\mathbf{x}})}\cdot\Big(\widehat{\nabla}\varphi(\xi,\hat{\mathbf{x}})\Big)\overline{\frac{\partial}{\partial\xi}\psi(\xi,\hat{\mathbf{x}})}\,d(\xi,\hat{\mathbf{x}}) && \text{(A.1g)}\\
& - \frac{\alpha}{\gamma-i\omega}\int_{\mathbb{R}_{>0}\times\Gamma} \frac{\xi\,\mathbf{v}(\hat{\mathbf{x}})}{\mathbf{n}(\hat{\mathbf{x}})\cdot\mathbf{v}(\hat{\mathbf{x}})}\cdot\Big(\widehat{\nabla}\varphi(\xi,\hat{\mathbf{x}})\Big)\overline{\frac{\partial}{\partial\xi}\psi(\xi,\hat{\mathbf{x}})}\,d(\xi,\hat{\mathbf{x}}) && \text{(A.1h)}\\
& - \int_{\mathbb{R}_{>0}\times\Gamma} \frac{(1+\xi)\,\mathbf{v}(\hat{\mathbf{x}})}{\mathbf{n}(\hat{\mathbf{x}})\cdot\mathbf{v}(\hat{\mathbf{x}})}\left(\frac{\partial}{\partial\xi}\varphi(\xi,\hat{\mathbf{x}})\right)\overline{\widehat{\nabla}\psi(\xi,\hat{\mathbf{x}})}\,d(\xi,\hat{\mathbf{x}}) && \text{(A.1i)}\\
& - \frac{\alpha}{\gamma-i\omega}\int_{\mathbb{R}_{>0}\times\Gamma} \frac{\xi\,\mathbf{v}(\hat{\mathbf{x}})}{\mathbf{n}(\hat{\mathbf{x}})\cdot\mathbf{v}(\hat{\mathbf{x}})}\left(\frac{\partial}{\partial\xi}\varphi(\xi,\hat{\mathbf{x}})\right)\overline{\widehat{\nabla}\psi(\xi,\hat{\mathbf{x}})}\,d(\xi,\hat{\mathbf{x}}) && \text{(A.1j)}\\
& - \frac{1}{2}\int_{\mathbb{R}_{>0}\times\Gamma} \frac{\mathbf{v}(\hat{\mathbf{x}})}{\mathbf{n}(\hat{\mathbf{x}})\cdot\mathbf{v}(\hat{\mathbf{x}})}\cdot\widehat{\nabla}\big(\varphi(\xi,\hat{\mathbf{x}})\,\overline{\psi(\xi,\hat{\mathbf{x}})}\big)\,d(\xi,\hat{\mathbf{x}}) && \text{(A.1k)}\\
& - \frac{1}{2}\frac{\alpha}{\gamma-i\omega}\int_{\mathbb{R}_{>0}\times\Gamma} \frac{\mathbf{v}(\hat{\mathbf{x}})}{\mathbf{n}(\hat{\mathbf{x}})\cdot\mathbf{v}(\hat{\mathbf{x}})}\cdot\widehat{\nabla}\big(\varphi(\xi,\hat{\mathbf{x}})\,\overline{\psi(\xi,\hat{\mathbf{x}})}\big)\,d(\xi,\hat{\mathbf{x}}) && \text{(A.1l)}\\
& + \int_{\mathbb{R}_{>0}\times\Gamma} \frac{\|\mathbf{v}(\hat{\mathbf{x}})\|^2}{\mathbf{n}(\hat{\mathbf{x}})\cdot\mathbf{v}(\hat{\mathbf{x}})}\Big(\widehat{\nabla}\varphi(\xi,\hat{\mathbf{x}})\Big)^{\top}\cdot\overline{\widehat{\nabla}\psi(\xi,\hat{\mathbf{x}})}\,d(\xi,\hat{\mathbf{x}}) && \text{(A.1m)}\\
& + \frac{\alpha}{\gamma-i\omega}\int_{\mathbb{R}_{>0}\times\Gamma} \frac{\|\mathbf{v}(\hat{\mathbf{x}})\|^2}{\mathbf{n}(\hat{\mathbf{x}})\cdot\mathbf{v}(\hat{\mathbf{x}})}\Big(\widehat{\nabla}\varphi(\xi,\hat{\mathbf{x}})\Big)^{\top}\cdot\overline{\widehat{\nabla}\psi(\xi,\hat{\mathbf{x}})}\,d(\xi,\hat{\mathbf{x}}) && \text{(A.1n)}\\
& - \frac{1}{2}\int_{\Gamma} \frac{1}{\mathbf{n}(\hat{\mathbf{x}})\cdot\mathbf{v}(\hat{\mathbf{x}})}\mathrm{tr}_{\Gamma}\varphi(\hat{\mathbf{x}})\,\overline{\mathrm{tr}_{\Gamma}\psi(\hat{\mathbf{x}})}\,d\hat{\mathbf{x}} && \text{(A.1o)}\\
& + (-i\omega)^2\int_{\mathbb{R}_{>0}\times\Gamma} (1+2\xi+\xi^2)\mathbf{n}(\hat{\mathbf{x}})\cdot\mathbf{v}(\hat{\mathbf{x}})\,\varphi(\xi,\hat{\mathbf{x}})\,\overline{\psi(\xi,\hat{\mathbf{x}})}\,d(\xi,\hat{\mathbf{x}}) && \text{(A.1p)}\\
& + (-i\omega)^2\frac{\alpha}{\gamma-i\omega}\int_{\mathbb{R}_{>0}\times\Gamma} (1+4\xi+3\xi^2)\mathbf{n}(\hat{\mathbf{x}})\cdot\mathbf{v}(\hat{\mathbf{x}})\,\varphi(\xi,\hat{\mathbf{x}})\,\overline{\psi(\xi,\hat{\mathbf{x}})}\,d(\xi,\hat{\mathbf{x}}) && \text{(A.1q)}\\
& + (-i\omega)^2\frac{\alpha^2}{(\gamma-i\omega)^2}\int_{\mathbb{R}_{>0}\times\Gamma} (2\xi+3\xi^2)\mathbf{n}(\hat{\mathbf{x}})\cdot\mathbf{v}(\hat{\mathbf{x}})\,\varphi(\xi,\hat{\mathbf{x}})\,\overline{\psi(\xi,\hat{\mathbf{x}})}\,d(\xi,\hat{\mathbf{x}}) && \text{(A.1r)}\\
& + (-i\omega)^2\frac{\alpha^3}{(\gamma-i\omega)^3}\int_{\mathbb{R}_{>0}\times\Gamma} \xi^2\mathbf{n}(\hat{\mathbf{x}})\cdot\mathbf{v}(\hat{\mathbf{x}})\,\varphi(\xi,\hat{\mathbf{x}})\,\overline{\psi(\xi,\hat{\mathbf{x}})}\,d(\xi,\hat{\mathbf{x}}) && \text{(A.1s)}
\end{aligned}
$$

## A.5. Exterior parts of adapted complex scaled sesquilinearform

$$\tilde{m}^{\sigma}_{\mathrm{ext}}(\omega)((\varphi,\psi),(\mathbf{h},\mathbf{g})) := \int_{\mathbb{R}_{>0}\times\Gamma} \frac{1}{\mathbf{n}(\hat{\mathbf{x}})\cdot\mathbf{v}(\hat{\mathbf{x}})}\frac{\partial}{\partial\xi}\varphi(\xi,\hat{\mathbf{x}})\overline{\frac{\partial}{\partial\xi}\psi(\xi,\hat{\mathbf{x}})}\,d(\xi,\hat{\mathbf{x}}) \tag{A.2a}$$

$$- \int_{\mathbb{R}_{>0}\times\Gamma} \frac{1}{\mathbf{n}(\hat{\mathbf{x}})\cdot\mathbf{v}(\hat{\mathbf{x}})}\frac{\partial}{\partial\xi}h_6(\xi,\hat{\mathbf{x}})\overline{\frac{\partial}{\partial\xi}\psi(\xi,\hat{\mathbf{x}})}\,d(\xi,\hat{\mathbf{x}}) \tag{A.2b}$$

$$+ \int_{\mathbb{R}_{>0}\times\Gamma} \frac{2\xi+\xi^2}{\mathbf{n}(\hat{\mathbf{x}})\cdot\mathbf{v}(\hat{\mathbf{x}})}\frac{\partial}{\partial\xi}\varphi(\xi,\hat{\mathbf{x}})\overline{\frac{\partial}{\partial\xi}\psi(\xi,\hat{\mathbf{x}})}\,d(\xi,\hat{\mathbf{x}}) \tag{A.2c}$$

$$+ \int_{\mathbb{R}_{>0}\times\Gamma} \frac{\xi^2}{\mathbf{n}(\hat{\mathbf{x}})\cdot\mathbf{v}(\hat{\mathbf{x}})}\frac{\partial}{\partial\xi}h_1(\xi,\hat{\mathbf{x}})\overline{\frac{\partial}{\partial\xi}\psi(\xi,\hat{\mathbf{x}})}\,d(\xi,\hat{\mathbf{x}}) \tag{A.2d}$$

$$- \frac{1}{4}\int_{\mathbb{R}_{>0}\times\Gamma} \frac{1}{\mathbf{n}(\hat{\mathbf{x}})\cdot\mathbf{v}(\hat{\mathbf{x}})}\varphi(\xi,\hat{\mathbf{x}})\,\overline{\psi(\xi,\hat{\mathbf{x}})}\,d(\xi,\hat{\mathbf{x}}) \tag{A.2e}$$

$$- \frac{1}{4}\int_{\mathbb{R}_{>0}\times\Gamma} \frac{1}{\mathbf{n}(\hat{\mathbf{x}})\cdot\mathbf{v}(\hat{\mathbf{x}})}h_1(\xi,\hat{\mathbf{x}})\,\overline{\psi(\xi,\hat{\mathbf{x}})}\,d(\xi,\hat{\mathbf{x}}) \tag{A.2f}$$

$$- \int_{\mathbb{R}_{>0}\times\Gamma} \frac{(1+\xi)\mathbf{v}(\hat{\mathbf{x}})}{\mathbf{n}(\hat{\mathbf{x}})\cdot\mathbf{v}(\hat{\mathbf{x}})}\cdot\left(\widehat{\nabla}\varphi(\xi,\hat{\mathbf{x}})\right)\overline{\frac{\partial}{\partial\xi}\psi(\xi,\hat{\mathbf{x}})}\,d(\xi,\hat{\mathbf{x}}) \tag{A.2g}$$

$$- \int_{\mathbb{R}_{>0}\times\Gamma} \frac{\xi\,\mathbf{v}(\hat{\mathbf{x}})}{\mathbf{n}(\hat{\mathbf{x}})\cdot\mathbf{v}(\hat{\mathbf{x}})}\cdot\left(\widehat{\nabla}h_1(\xi,\hat{\mathbf{x}})\right)\overline{\frac{\partial}{\partial\xi}\psi(\xi,\hat{\mathbf{x}})}\,d(\xi,\hat{\mathbf{x}}) \tag{A.2h}$$

$$- \int_{\mathbb{R}_{>0}\times\Gamma} \frac{(1+\xi)\,\mathbf{v}(\hat{\mathbf{x}})}{\mathbf{n}(\hat{\mathbf{x}})\cdot\mathbf{v}(\hat{\mathbf{x}})}\left(\frac{\partial}{\partial\xi}\varphi(\xi,\hat{\mathbf{x}})\right)\overline{\widehat{\nabla}\psi(\xi,\hat{\mathbf{x}})}\,d(\xi,\hat{\mathbf{x}}) \tag{A.2i}$$

$$- \int_{\mathbb{R}_{>0}\times\Gamma} \frac{\xi\,\mathbf{v}(\hat{\mathbf{x}})}{\mathbf{n}(\hat{\mathbf{x}})\cdot\mathbf{v}(\hat{\mathbf{x}})}\left(\frac{\partial}{\partial\xi}h_1(\xi,\hat{\mathbf{x}})\right)\overline{\widehat{\nabla}\psi(\xi,\hat{\mathbf{x}})}\,d(\xi,\hat{\mathbf{x}}) \tag{A.2j}$$

$$- \frac{1}{2}\int_{\mathbb{R}_{>0}\times\Gamma} \frac{\mathbf{v}(\hat{\mathbf{x}})}{\mathbf{n}(\hat{\mathbf{x}})\cdot\mathbf{v}(\hat{\mathbf{x}})}\cdot\widehat{\nabla}\left(\varphi(\xi,\hat{\mathbf{x}})\,\overline{\psi(\xi,\hat{\mathbf{x}})}\right)d(\xi,\hat{\mathbf{x}}) \tag{A.2k}$$

$$- \frac{1}{2}\int_{\mathbb{R}_{>0}\times\Gamma} \frac{\mathbf{v}(\hat{\mathbf{x}})}{\mathbf{n}(\hat{\mathbf{x}})\cdot\mathbf{v}(\hat{\mathbf{x}})}\cdot\widehat{\nabla}\left(h_1(\xi,\hat{\mathbf{x}})\,\overline{\psi(\xi,\hat{\mathbf{x}})}\right)d(\xi,\hat{\mathbf{x}}) \tag{A.2l}$$

$$+ \int_{\mathbb{R}_{>0}\times\Gamma} \frac{\|\mathbf{v}(\hat{\mathbf{x}})\|^2}{\mathbf{n}(\hat{\mathbf{x}})\cdot\mathbf{v}(\hat{\mathbf{x}})}\left(\widehat{\nabla}\varphi(\xi,\hat{\mathbf{x}})\right)^{\top}\cdot\overline{\widehat{\nabla}\psi(\xi,\hat{\mathbf{x}})}\,d(\xi,\hat{\mathbf{x}}) \tag{A.2m}$$

$$+ \int_{\mathbb{R}_{>0}\times\Gamma} \frac{\|\mathbf{v}(\hat{\mathbf{x}})\|^2}{\mathbf{n}(\hat{\mathbf{x}})\cdot\mathbf{v}(\hat{\mathbf{x}})}\left(\widehat{\nabla}h_1(\xi,\hat{\mathbf{x}})\right)^{\top}\cdot\overline{\widehat{\nabla}\psi(\xi,\hat{\mathbf{x}})}\,d(\xi,\hat{\mathbf{x}}) \tag{A.2n}$$

$$- \frac{1}{2}\int_{\Gamma} \frac{1}{\mathbf{n}(\hat{\mathbf{x}})\cdot\mathbf{v}(\hat{\mathbf{x}})}\mathrm{tr}_{\Gamma}\varphi(\mathbf{x})\,\overline{\mathrm{tr}_{\Gamma}\psi(\hat{\mathbf{x}})}\,d\hat{\mathbf{x}} \tag{A.2o}$$

$$+ \int_{\mathbb{R}_{>0}\times\Gamma} (\gamma h_1(\xi,\hat{\mathbf{x}}) - \alpha\varphi(\xi,\hat{\mathbf{x}}))\overline{g_1(\xi,\hat{\mathbf{x}})}\,d(\xi,\hat{\mathbf{x}}) \tag{A.2p}$$

$$+ \int_{\mathbb{R}_{>0}\times\Gamma} h_2(\xi,\hat{\mathbf{x}})\overline{g_2(\xi,\hat{\mathbf{x}})}\,d(\xi,\hat{\mathbf{x}}) \tag{A.2q}$$

$$+ \int_{\mathbb{R}_{>0}\times\Gamma} (\gamma h_3(\xi,\hat{\mathbf{x}}) - \alpha h_2(\xi,\hat{\mathbf{x}}))\overline{g_3(\xi,\hat{\mathbf{x}})}d(\xi,\hat{\mathbf{x}}) \tag{A.2r}$$

$$+ \int_{\mathbb{R}_{>0}\times\Gamma} (\gamma h_4(\xi,\hat{\mathbf{x}}) - \alpha h_3(\xi,\hat{\mathbf{x}}))\overline{g_4(\xi,\hat{\mathbf{x}})}d(\xi,\hat{\mathbf{x}}) \tag{A.2s}$$

$$+ \int_{\mathbb{R}_{>0}\times\Gamma} h_5(\xi,\hat{\mathbf{x}})\overline{g_5(\xi,\hat{\mathbf{x}})}d(\xi,\hat{\mathbf{x}}) \tag{A.2t}$$

$$+ \int_{\mathbb{R}_{>0}\times\Gamma} (\gamma+\alpha)h_6(\xi,\hat{\mathbf{x}}) - \alpha\overline{g_6(\xi,\hat{\mathbf{x}})}d(\xi,\hat{\mathbf{x}}), \tag{A.2u}$$

$$\tilde{s}^{\sigma}_{\mathrm{ext}}(\omega)((\varphi,\psi),(\mathbf{h},\mathbf{g})) := \tag{A.3a}$$

$$+\int_{\mathbb{R}_{>0}\times\Gamma}(1+2\xi+\xi^2)\mathbf{n}(\hat{\mathbf{x}})\cdot\mathbf{v}(\hat{\mathbf{x}})\,h_5(\xi,\hat{\mathbf{x}})\,\overline{\psi(\xi,\hat{\mathbf{x}})}\,d(\xi,\hat{\mathbf{x}}) \tag{A.3b}$$

$$+\int_{\mathbb{R}_{>0}\times\Gamma}(1+4\xi+3\xi^2)\mathbf{n}(\hat{\mathbf{x}})\cdot\mathbf{v}(\hat{\mathbf{x}})\,h_2(\xi,\hat{\mathbf{x}})\,\overline{\psi(\xi,\hat{\mathbf{x}})}\,d(\xi,\hat{\mathbf{x}}) \tag{A.3c}$$

$$+\int_{\mathbb{R}_{>0}\times\Gamma}(2\xi+3\xi^2)\mathbf{n}(\hat{\mathbf{x}})\cdot\mathbf{v}(\hat{\mathbf{x}})\,h_3(\xi,\hat{\mathbf{x}})\,\overline{\psi(\xi,\hat{\mathbf{x}})}\,d(\xi,\hat{\mathbf{x}}) \tag{A.3d}$$

$$+\int_{\mathbb{R}_{>0}\times\Gamma}\xi^2\mathbf{n}(\hat{\mathbf{x}})\cdot\mathbf{v}(\hat{\mathbf{x}})\,h_4(\xi,\hat{\mathbf{x}})\,\overline{\psi(\xi,\hat{\mathbf{x}})}\,d(\xi,\hat{\mathbf{x}}) \tag{A.3e}$$

$$+\int_{\mathbb{R}_{>0}\times\Gamma}(h_1(\xi,\hat{\mathbf{x}})\overline{g_1(\xi,\hat{\mathbf{x}})}\,d(\xi,\hat{\mathbf{x}}) \tag{A.3f}$$

$$-\int_{\mathbb{R}_{>0}\times\Gamma}h_1(\xi,\hat{\mathbf{x}}))\overline{g_2(\xi,\hat{\mathbf{x}})}\,d(\xi,\hat{\mathbf{x}}) \tag{A.3g}$$

$$+\int_{\mathbb{R}_{>0}\times\Gamma}h_3(\xi,\hat{\mathbf{x}}))\overline{g_3(\xi,\hat{\mathbf{x}})}d(\xi,\hat{\mathbf{x}}) \tag{A.3h}$$

$$+\int_{\mathbb{R}_{>0}\times\Gamma}(h_4(\xi,\hat{\mathbf{x}})\overline{g_4(\xi,\hat{\mathbf{x}})}d(\xi,\hat{\mathbf{x}}) \tag{A.3i}$$

$$-\int_{\mathbb{R}_{>0}\times\Gamma}\varphi(\xi,\hat{\mathbf{x}}))\overline{g_5(\xi,\hat{\mathbf{x}})}d(\xi,\hat{\mathbf{x}}) \tag{A.3j}$$

$$+\int_{\mathbb{R}_{>0}\times\Gamma}h_6(\xi,\hat{\mathbf{x}})\overline{g_6(\xi,\hat{\mathbf{x}})}d(\xi,\hat{\mathbf{x}}) \tag{A.3k}$$

with $(\mathbf{h},\mathbf{g}) := (h_1,g_1,h_2,g_2,h_3,g_3,h_4,g_4,h_5,g_5,h_6,g_6)$.

# Bibliography


[Ber94] J.-P. Berenger. A perfectly matched layer for the absorption of electromagnetic waves. *Journal of Computational Physics*, 114(2):185–200, 1994. DOI: https://doi.org/10.1006/jcph.1994.1159.

[BP13] J. H. Bramble and J. E. Pasciak. Analysis of a Cartesian PML approximation to acoustic scattering problems in R2 and R3. *Journal of Computational and Applied Mathematics*, 247:209–230, 2013. DOI: https://doi.org/10.1016/j.cam.2012.12.022.

[CK13] D. Colton and R. Kress. *Inverse acoustic and electromagnetic scattering theory*. New York, NY: Springer, 3rd ed. Edition, 2013. DOI: 10.1007/978-1-4614-4942-3. URL: cds.cern.ch/record/1499488.

[Eva10] L. C. Evans. *Partial differential equations*. Providence, RI: American Mathematical Society (AMS), 2nd ed. Edition, 2010.

[Hal19] M. Halla. *Analysis of Radial Complex Scaling Methods for Scalar Resonance Problems in Open Systems*. PhD thesis, Technische Universität Wien, Vienna, Austria, 2019. DOI: 10.34726/hss.2019.69603. URL: https://repositum.tuwien.at/handle/20.500.12708/11464.

[Hal21] M. Halla. Analysis of Radial Complex Scaling Methods: Scalar Resonance Problems. *SIAM Journal on Numerical Analysis*, 59(4):2054–2074, 2021. DOI: 10.1137/20M1354234. eprint: https://doi.org/10.1137/20M1354234.

[HKW24] M. Halla, M. Kachanovska, and M. Wess. Radial perfectly matched layers and infinite elements for the anisotropic wave equation. 2024. URL: https://hal.science/hal-04419377.

[IMN+25] M. Innerberger, J. M. Melenk, L. Nannen, D. Praetorius, and A. Rieder. Numerics of Differential Equations. https://tuwel.tuwien.ac.at/pluginfile.php/4300349/mod_resource/content/5/numodes.pdf, 2025.

[Joh21] S. G. Johnson. Notes on Perfectly Matched Layers (PMLs), 2021. arXiv: 2108.05348 [cs.CE]. URL: https://arxiv.org/abs/2108.05348.

[Jün23] A. Jüngel. Partielle Differentialgleichungen. https://www.tuwien.at/index.php?eID=dumpFile&t=f&f=188928&token=d67621b4438589a3ab582c7fac4b758d7891045b, 2023.

[MF24] J. M. Melenk and M. Faustmann. Numerics of partial differential equations: instationary problems. https://tuwel.tuwien.ac.at/pluginfile.php/4420919/mod_resource/content/2/fem2.pdf, 2024.

[NW22] L. Nannen and M. Wess. Complex-scaled infinite elements for resonance problems in heterogeneous open systems. *Advances in Computational Mathematics*, 48(2):8, 2022. DOI: 10.1007/s10444-021-09923-1.

[Obe90] F. Oberhettinger. *Tables of Fourier Transforms and Fourier Transforms of Distributions*. Springer, Berlin, Heidelberg, 1990. DOI: 10.1007/978-3-642-74349-8.

[RSS12] D. Ruprecht, A. Schädle, and F. Schmidt. Transparent boundary conditions based on the pole condition for time-dependent, two-dimensional problems. *Numerical Methods for Partial Differential Equations*, 29(4):1367–1390, 2012. DOI: 10.1002/num.21759.

[Sch14] J. Sch¨oberl. C++11 Implementation of Finite Elements in NGSolve. In 2014. URL: https://api.semanticscholar.org/CorpusID:214588478.

[Sch97] J. Schöberl. NETGEN - An advancing front 2D/3D-mesh generator based on abstract rules. *Computing and Visualization in Science*, 1997.

[Sim79] B. Simon. The definition of molecular resonance curves by the method of exterior complex scaling. *Physics Letters A*, 71(2-3):211–214, 1979. DOI: 10.1016/0375-9601(79)90503-9.

[Wes20] M. Wess. *Frequency-dependent complex-scaled infinite elements for exterior Helmholtz resonance problems*. Wien, 2020. DOI: https://doi.org/10.34726/hss.2020.78903. URL: https://repositum.tuwien.at/bitstream/20.500.12708/15095/2/Wess%20Markus%20-%202020%20-%20Frequency-dependent%20complex-scaled%20infinite%20elements%20for...pdf.